Inorganic Chemistry
Article

*Inorg. Chem.* **2010**, *49*, 8601–8619 **8601**
DOI: 10.1021/ic101220v

# Dimerization of Dendrimeric Lanthanide Complexes: Thermodynamic, Thermal, and Liquid-Crystalline Properties

**Thomas Binderup Jensen,[†] Emmanuel Terazzi,[†] Kerry-Lee Buchwalder,[†] Laure Guénée,[†] Homayoun Nozary,[†] Kurt Schenk,[‡] Benoît Heinrich,[§] Bertrand Donnio,[§] Daniel Guillon,[§] and Claude Piguet*[,†]**

[†]*Department of Inorganic, Analytical and Applied Chemistry, University of Geneva, 30 quai E. Ansermet, CH-1211 Geneva 4, Switzerland,* [§]*Groupe des Matériaux Organiques, Institut de Physique et Chimie des Matériaux de Strasbourg (IPCMS), 23 rue du Loess, B.P. 43, F67034 Strasbourg Cedex 2, France, and* [‡]*Laboratory of Crystallography, Ecole Polytechnique Fédérale de Lausanne, CH-1015 Lausanne, Switzerland*

Received June 18, 2010

A series of 10 different mesomorphic semidendrimeric tridentate ligands **L5**−**L14** grafted with terminal cyanobiphenyl groups have been synthesized. Upon reaction with $Ln(NO_3)_3$ (Ln = trivalent lanthanide), the central 2,6-bis(*N*-ethylbenzimidazol-2-yl)pyridine unit is meridionally tricoordinated to the metal to give rodlike monomeric $[Ln(\mathbf{L}\boldsymbol{k})(NO_3)_3]$ and H-shaped dimeric $[Ln_2(\mathbf{L}\boldsymbol{k})_2(NO_3)_6]$ complexes. For the small $Lu^{III}$ cation, the monomeric complexes are quantitatively formed in a noncoordinating $CD_2Cl_2$ solution. For larger cations (Ln = Eu, Pr), the thermodynamic equilibrium $2[Ln(\mathbf{L}\boldsymbol{k})(NO_3)_3] \leftrightarrow [Ln_2(\mathbf{L}\boldsymbol{k})_2(NO_3)_6]$ can be evidenced across the complete ligand series. Detailed thermodynamic studies show that the dimeric complexes result from the formation of primary intermetallic nitrate bridges whose strength depends on the metallic size. For each complex, secondary nonspecific interstrand van der Waals interactions produce nonartifactual enthalpy/entropy compensation. In the absence of solvent, only the complexes with the most extended ligands **L5** and **L6** produce thermotropic mesophases. Layered organizations are dominant (smectic A) with the induction of nematogenic behavior at high temperature when interstrand interactions are modulated by methyl substitutions. Correlations between the trend of dimerization and the sequences of thermotropic mesophases are attempted.

## Introduction

Thermotropic liquid crystals are usually produced by the melting of amphiphilic molecules possessing a rigid polarizable aromatic core grafted with long and flexible alkyl chains. Optimization of the intermolecular interactions in the crystalline state results in a microsegregation process, in which the rigid cores are packed together, while the less polarizable flexible alkyl chains fill the residual voids of the structure.[1] Upon heating, decorrelation between the flexible alkyl chains produces a molten continuum, in which the clusters of interacting rigid cores are dispersed, thus forming what is known as a thermotropic mesophase. When the incriminated amphiphilic molecule contains a metallic center, i.e., a metallomesogen, the considerable three-dimensional expansion brought by the coordination sphere of the metal seriously disturbs intermolecular interactions, and successful microsegregation was originally induced for rodlike two-coordinate or disklike square-planar four-coordinate metallic complexes.[2] Only a few metallomesogens have either a tetrahedral[3] or an octahedral[4] metal center, because these coordination geometries are difficult to combine with the requirement of structural anisotropy and efficient intermolecular interactions

*To whom correspondence should be addressed. E-mail: Claude.Piguet@unige.ch.

(1) (a) Guillon, D.; Skoulios, A. *J. Phys.* (*Paris*) **1976**, *37*, 797–800. (b) Skoulios, A.; Guillon, D. *Mol. Cryst. Liq. Cryst.* **1988**, *165*, 317–332.

(2) (a) Giroud-Godquin, A. M.; Maitlis, P. M. *Angew. Chem., Int. Ed. Engl.* **1991**, *30*, 375–402. (b) Bruce, D. W. *J. Chem. Soc., Dalton Trans.* **1993**, 2983–2989. (c) Hudson, S. A.; Maitlis, P. M. *Chem. Rev.* **1993**, *93*, 861–885. (d) Serrano, J. L. *Metallomesogens, Synthesis, Properties and Applications*; VCH: Weinheim, Germany, 1996. (e) Donnio, B.; Bruce, D. W. *Struct. Bonding* (*Berlin*) **1999**, *95*, 194–247. (f) Donnio, B.; Guillon, D.; Deschenaux, R.; Bruce, D. W. In *Comprehensive Coordination Chemistry*; McCleverty, J. A., Meyer, T. J., Eds.; Elsevier: Oxford, U.K., 2003; Vol. 7, Chapter 79. (g) Date, R. W.; Fernandez Iglesias, E.; Rowe, K. E.; Elliott, J. M.; Bruce, D. W. *Dalton Trans.* **2003**, 1914–1931.

(3) (a) Neve, F.; Ghedini, M.; De Munno, G.; Levelut, A. M. *Chem. Mater.* **1995**, *7*, 688–693. (b) Douce, L.; El-ghayouri, A.; Skoulios, A.; Ziessel, R. *Chem. Commun.* **1999**, 2033–2034. (c) Giménez, R.; Manrique, A. B.; Uriel, S.; Barbera, J.; Serrano, J. L. *Chem. Commun.* **2004**, 2064–2065. (d) Cavero, E.; Uriel, S.; Romero, P.; Serrano, J. L.; Giménez, R. *J. Am. Chem. Soc.* **2007**, *129*, 11698–11618.

(4) (a) Lattermann, G.; Schmidt, S.; Kleppinger, R.; Wendorf, J. H. *Adv. Mater.* **1992**, *4*, 30–33. (b) Zheng, H.; Swager, T. M. *J. Am. Chem. Soc.* **1994**, *116*, 761–762. (c) Swager, T. M.; Zheng, H. *Mol. Cryst. Liq. Cryst.* **1995**, *260*, 301–306. (d) Bruce, D. W.; Liu, X. H. *Liq. Cryst.* **1995**, *18*, 165–166. (e) Liu, X.-H.; Abser, M. N.; Bruce, D. W. *J. Organomet. Chem.* **1998**, *551*, 271–280. (f) Walf, G. H.; Benda, R.; Litterst, F. J.; Stebani, U.; Schmidt, S.; Lattermann, G. *Chem.—Eur. J.* **1998**, *4*, 93–99. (g) Rowe, K. E.; Bruce, D. W. *J. Chem. Soc., Dalton Trans.* **1996**, 3913–3915. (h) Morrone, S.; Guillon, D.; Bruce, D. W. *Inorg. Chem.* **1996**, *35*, 7041–7048.


Published on Web 08/18/2010

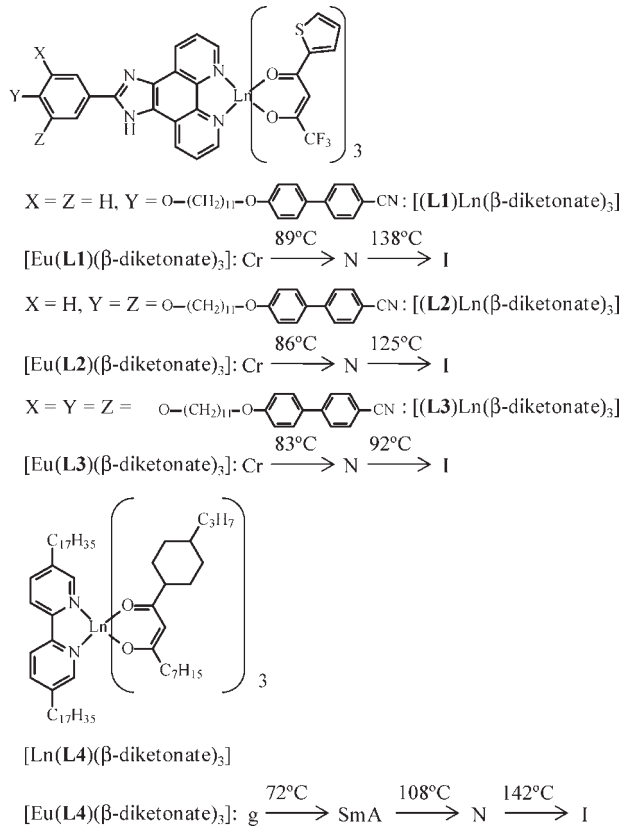


**Figure 1.** Chemical structures of the nematogenic complexes [Ln(**L*k***)(*β*-diketonate)$_3$] (**L*k*** = **L1**−**L4**). The phase sequences and transition temperatures are given for Ln = Eu as a typical example (g = glass, Cr = crystal, SmA = smectic A, N = nematic, and I = isotropic liquid).[8].

compatible with the formation of a mesophase. Because of stronger geometrical constraints, it is even more difficult to obtain metallomesogens with coordination numbers larger than 6, and the number of systems providing thermotropic lanthanide-containing mesophases (i.e., lanthanidomesogens) remains limited.[5,6] Roughly speaking, rodlike salicylaldimine Schiff bases (or closely related bidentate ligands) coordinated to trivalent lanthanides yield lamellar smectic phases, while disklike polysubstituted phthalocyanine sandwich complexes or polycatenar complexes give columnar and cubic mesophases.[5,6] Despite its suitability for practical applications,[7] the fluid nematic organization has been rarely observed for thermotropic lanthanidomesogens,[8] and a rational approach

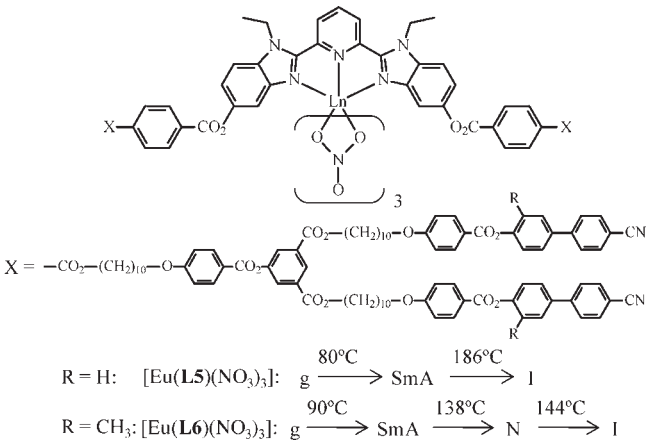


**Figure 2.** Chemical structures and mesogenic behaviors of the symmetrical dendrimeric complexes [Ln(**L*k***)(NO$_3$)$_3$] (**L*k*** = **L5** and **L6**). The phase sequences and transition temperatures are given for Ln = Eu as a typical example (g = glass, SmA = smectic A, N = nematic, and I = isotropic liquid).[10b].

for these materials remains to be developed. To the best of our knowledge and if we exclude the lanthanide doping of commercially available nematic mesogens,[7] the complexes [Ln(**L*k***)(*β*-diketonate)$_3$] (**L*k*** = **L1**−**L4**) are the only lanthanide-containing compounds exhibiting thermotropic nematic mesophases over a temperature domain larger than 10° (Figure 1).[8] As a guideline for inducing nematogenic behavior, the authors introduced some unsymmetrical coordinated ligands in the complexes [Ln(**L*k***)(*β*-diketonate)$_3$] that are expected to destabilize the residual lateral interactions responsible for the formation of layers in smectic mesophases (Figure 1).[8] Parallel contributions by Deschenaux and coworkers aiming at the encapsulation of bulky isotropic fullerene into nematic mesophases indeed reach the same conclusion with the introduction of a large carbone allotrope into unsymmetrical dendrimers.[9]

Inspired by this reasoning, we suspected that nematic lanthanidomesogens may also be induced by using symmetrical complexes according to the fact that the periodic organization found in the smectic phase is disrupted by specific substitutions that hinder lateral stacking interactions. The dendrimeric receptor **L5** was originally designed for inducing calamitic mesomorphism in thermotropic lanthanidomesogens thanks to the connection of four terminal cyanobiphenyl smectogenic units (Figure 2).[10] The nitrato complexes [Ln(**L5**)(NO$_3$)$_3$] indeed forms smectic A mesophases in the 80−180 °C temperature range with the heavier lanthanides (Ln = Eu−Lu).[10b] Building on these preliminary observations, we showed that the simple introduction of methyl groups within the cyanobiphenyl units in **L6** seemed to destabilize the smectic A organization, and a nematic mesophase could be observed over a few degrees prior to isotropization for the symmetrical complexes [Ln(**L6**)(NO$_3$)$_3$] (Ln = Eu, Lu; Figure 2).[11]

(5) For comprehensive reviews, see: (a) Binnemans, K.; Görller-Walrand, C. *Chem. Rev.* **2002**, *102*, 2303–2346. (c) Piguet, C.; Bünzli, J.-C. G.; Donnio, B.; Guillon, D. *Chem. Commun.* **2006**, 3755–3768.

(6) For recent reports on lanthanido- and actinidomesogens, see: (a) Sessler, J. L.; Melfi, P. J.; Tomat, E.; Callaway, W.; Huggins, M. T.; Gordon, P. L.; Webster, K. D.; Date, R. W.; Bruce, D. W.; Donnio, B. *J. Alloys Compd.* **2006**, *418*, 171–177. (b) Binnemans, K.; Lodewyckx, K.; Cardinaels, T.; Parac-Vogt, T. N.; Bourgogne, C.; Guillon, D.; Donnio, B. *Eur. J. Inorg. Chem.* **2006**, 150–157. (c) Cardinaels, T.; Ramaekers, J.; Nockemann, P.; Driesen, K.; Van Hecke, K.; Van Meervelt, L.; Lei, S.; De Feyter, S.; Guillon, D.; Donnio, B.; Binnemans, K. *Chem. Mater.* **2008**, *20*, 1278–1291.

(7) (a) van Deun, R.; De Fré, B.; Moors, D.; Binnemans, K. *J. Mater. Chem.* **2003**, *13*, 1520–1522. (b) Driesen, K.; Moors, D.; Beeckman, J.; Neyts, K.; Görller-Walrand, C.; Binnemans, K. *J. Luminesc.* **2007**, *127*, 611–615 and references therein.

(8) (a) Cardinaels, T.; Driesen, K.; Parac-Vogt, T. N.; Heinrich, B.; Bourgogne, C.; Guillon, D.; Donnio, B.; Binnemans, K. *Chem. Mater.* **2005**, *17*, 6589–6598. (b) Galyametdinov, Y. G.; Knyazev, A. A.; Dzhabarov, V. I.; Cardinaels, T.; Driesen, K.; Görller-Walrand, C.; Binnemans, K. *Adv. Mater.* **2008**, *20*, 252–257.

(9) (a) Deschenaux, R.; Donnio, B.; Guillon, D. *New J. Chem.* **2007**, *31*, 1064–1073. (b) Lenoble, J.; Campidelli, S.; Maringa, N.; Donnio, B.; Guillon, D.; Yevlampieva, N.; Deschenaux, R. *J. Am. Chem. Soc.* **2007**, *129*, 9941–9952.

(10) (a) Dardel, B.; Guillon, D.; Heinrich, B.; Deschenaux, R. *J. Mater. Chem.* **2001**, *11*, 2814–2831. (b) Campidelli, S.; Lenoble, J.; Barbera, J.; Paolucci, F.; Marcaccio, M.; Paolucci, D.; Deschenaux, R. *Macromolecules* **2005**, *38*, 7915–7925. (c) Terazzi, E.; Bocquet, B.; Campidelli, S.; Donnio, B.; Guillon, D.; Deschenaux, R.; Piguet, C. *Chem. Commun.* **2006**, 2922–2924.

(11) Jensen, T. B.; Terazzi, E.; Donnio, B.; Guillon, D.; Piguet, C. *Chem. Commun.* **2008**, 181–183.

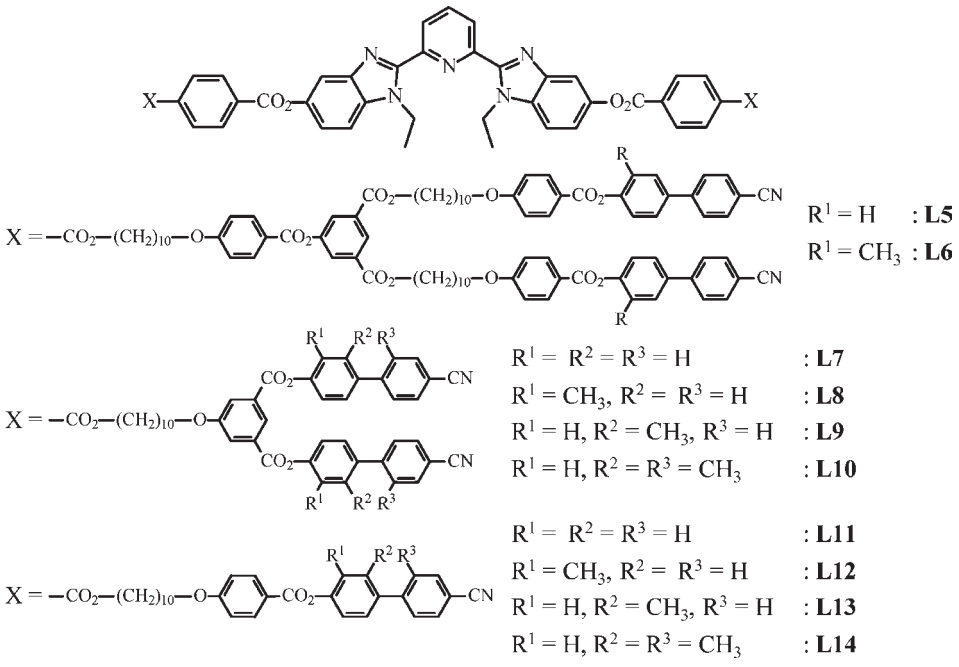


**Figure 3.** Chemical structures of the symmetrical ligands **L5**−**L14** considered in this contribution.

Interestingly, parallel studies of these molecular complexes dissolved in noncoordinating dichloromethane showed that dimerization [equilibrium (1)] is a key characteristic whose free-energy change depends on both the lanthanide size and ligand substitution, thus offering some potential modulations of the global shapes and geometries of the starting complexes for the design of lanthanidomesogens.

$$2[\mathrm{Ln}(\mathbf{L}k)(\mathrm{NO_3})_3] \rightleftharpoons [\mathrm{Ln_2}(\mathbf{L}k)_2(\mathrm{NO_3})_6] \quad \beta_{\mathrm{dim}}^{\mathrm{Ln},\,\mathbf{L}k} \qquad (1)$$

In this contribution, we report on the systematic thermodynamic investigation of the effect of chain lengths, of chain branching, of methyl substitutions, and of metallic size on the formation of the monomeric $[\mathrm{Ln}(\mathbf{L}k)(\mathrm{NO_3})_3]$ and dimeric $[\mathrm{Ln_2}(\mathbf{L}k)_2(\mathrm{NO_3})_6]$ complexes in solution with a collection of 10 ligands **L5**−**L14** and two lanthanides Ln = Pr and Eu (Figure 3). The thermal properties of the mesogenic complexes $[\mathrm{Ln}(\mathbf{L5})(\mathrm{NO_3})_3]$ and $[\mathrm{Ln}(\mathbf{L6})(\mathrm{NO_3})_3]$ are tentatively rationalized in light of their affinity for dimerization in a noncoordinating solvent.

## Results and Discussion

**Syntheses and Characterization of Ligands L5−L14 and of Their Complexes $[\mathrm{Ln}(\mathbf{L}k)(\mathrm{NO_3})_3]$ ($\mathbf{L}k$ = L5−L14 and Ln = La, Pr, Eu, Tb, Gd, Lu, Y).** The syntheses of the symmetrical ligands **L5** and **L6** follow a linear strategy, in which the formations of ester bonds via activation with carbodiimides (DCC or EDCI) alternate with carboxylate and hydroxyl deprotection reactions (Schemes 1 and S1 and S2 in the Supporting Information).[10,11] Because of the tedious synthetic procedure leading to the final dendrimeric ligand **L5** (16 steps), a single methyl-substituted analogue **L6** (17 steps) has been synthesized (family 1, Scheme 1), while two groups of smaller ligands with four different methyl-substituted cyanobiphenyls have been designed (family 2, short and branched ligands **L7**−**L10**, Scheme S1 in the Supporting Information, 12 steps; family 3, short and linear ligands **L11**−**L14**, Scheme S2 in the Supporting Information, 12 steps).

The selective introduction of methyl groups into the cyanobiphenyl units **1**−**3** follows a Miyaura−Suzuki strategy,[12] in which (4-cyanophenyl)boronic acid or (4-cyano-2-methylphenyl)boronic acid[13] is coupled with adequate halomethylphenols (Scheme 2).

All ligands **L5**−**L14** gave satisfying elemental analyses, displayed molecular peaks by electrospray ionization mass spectrometry (ESI-MS) corresponding to $[\mathbf{L}k + \mathrm{H}]^+$, and provided $^1$H NMR spectra typical for $C_{2v}$-symmetrical organization with a trans−trans conformation of the central tridentate 2,6-bis(benzimidazole)pyridine unit (Figure 4a). The reaction of stoichiometric amounts of $\mathbf{L}k$ with $\mathrm{Ln(NO_3)_3 \cdot}x\mathrm{H_2O}$ (Ln = La, Pr, Eu, Gd, Tb, Lu, Y; $x$ = 1−3) in acetonitrile/dichloromethane followed by evaporation yielded insoluble powders whose elemental analyses were compatible with the formation of complexes $[\mathrm{Ln}(\mathbf{L}k)(\mathrm{NO_3})_3]\cdot x\mathrm{H_2O}$ ($\eta$ = 72−89%; Table S1 in the Supporting Information). Except for the downfield shift of the $^1$H NMR signal of the proton attached to the para position of the central pyridine ring (H1), which is diagnostic for the meridional tricoordination of the bis(benzimidazole)pyridine binding unit to $\mathrm{Lu(NO_3)_3}$,[14,15] the $^1$H NMR spectra of the free ligands $\mathbf{L}k$ and of their diamagnetic complexes $[\mathrm{Lu}(\mathbf{L}k)(\mathrm{NO_3})_3]$ in $\mathrm{CDCl_3}$ are similar (Figure 4a,b). The detection of a single set of aromatic benzimidazole

(12) (a) Miyaura, N.; Suzuki, A. *Chem. Rev.* **1995**, *95*, 2457–2483. (b) Stanforth, S. P. *Tetrahedron* **1998**, *54*, 263–303. (c) Tobisu, M.; Chatani, N. *Angew. Chem., Int. Ed.* **2009**, *48*, 3565–3568.

(13) Stones, D.; Manky, S.; Lu, X.; Hall, D. G. *Chem.—Eur. J.* **2004**, *10*, 92–100.

(14) (a) Nozary, H.; Piguet, C.; Tissot, P.; Bernardinelli, G.; Bünzli, J.-C. G.; Deschenaux, R.; Guillon, D. *J. Am. Chem. Soc.* **1998**, *120*, 12274–12288. (b) Nozary, H.; Piguet, C.; Rivera, J.-P.; Tissot, P.; Bernardinelli, G.; Vulliermet, N.; Weber, J.; Bünzli, J.-C. G. *Inorg. Chem.* **2000**, *39*, 5286–5298. (c) Nozary, H.; Piguet, C.; Rivera, J.-P.; Tissot, P.; Morgantini, P.-Y.; Weber, J.; Bernardinelli, G.; Bünzli, J.-C. G.; Deschenaux, R.; Donnio, B.; Guillon, D. *Chem. Mater.* **2002**, *14*, 1075–1090.

(15) Terazzi, E.; Torelli, S.; Bernardinelli, G.; Rivera, J.-P.; Bénech, J.-M.; Bourgogne, C.; Donnio, B.; Guillon, D.; Imbert, D.; Bünzli, J.-C. G.; Pinto, A.; Jeannerat, D.; Piguet, C. *J. Am. Chem. Soc.* **2005**, *127*, 888–903.

**Scheme 1.** Synthesis of Ligands **L5** and **L6** (DCC = *N*,*N*′-Dicyclohexylcarbodiimide, DPTS = 4-[(Dimethylamino)pyridinium]-4-toluenesulfonate, 4-Ppy = 4-Pyrrolidinopyridine, DMAP = 4-(Dimethylamino)pyridine, EDCI = *N*-[3-(Dimethylamino)propyl]-*N*′-ethylcarbodiimide)

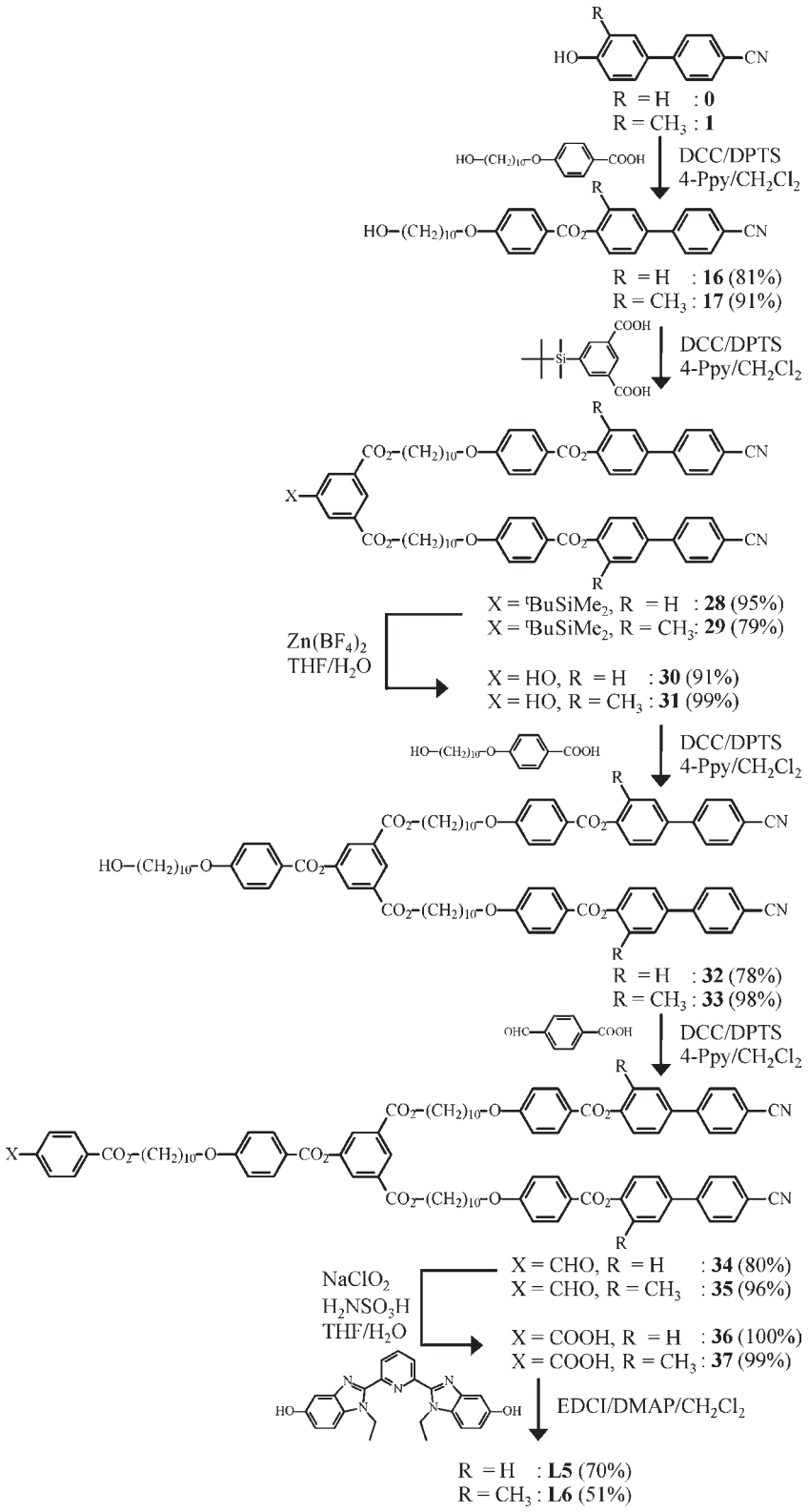


protons points to the existence of a 2-fold axis passing through the central pyridine ring. The concomitant observation of enantiotopic signals for the methylene groups implies additional symmetry planes compatible with a global $C_{2v}$ point group for both the ligand and its $Lu^{III}$ complex on the NMR time scale, a behavior previously well-documented for closely related complexes with polycatenar tridentate ligands **L15** and **L16** (see Figure 5 for the structures of these ligands).[14,15]

Beyond the expected opposite paramagnetic shifts brought by Ln = Pr ($4f^2$, spin expectation factor $\langle S_z \rangle_{Pr} = -2.97$, and Bleaney factor $C_{Pr} = -11.0$) or Ln = Eu

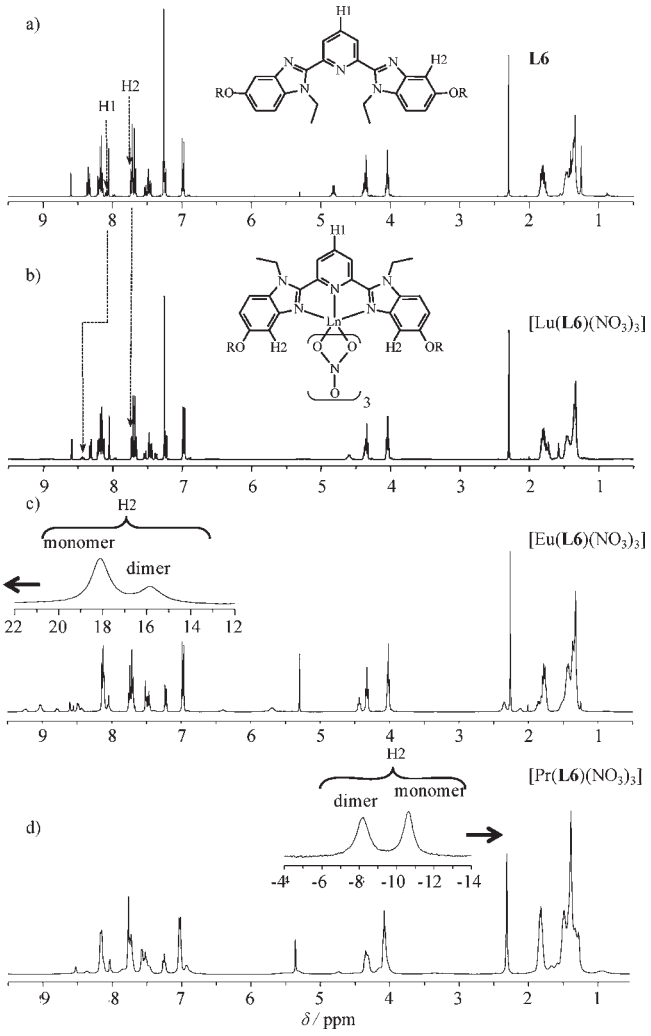


**Figure 4.** 400 MHz $^1$H NMR spectra of (a) **L6** and of their complexes ($CDCl_3$) (b) [Lu(**L6**)$(NO_3)_3$] ($CDCl_3$), (c) [Eu(**L6**)$(NO_3)_3$] ($CD_2Cl_2$), and (d) [Pr(**L6**)$(NO_3)_3$] ($CD_2Cl_2$).

($4f^6$, $\langle S_z\rangle_{Eu} = 10.68$, and $C_{Eu} = 4.0$),[16] which spread the $^1$H NMR signal over $-15 \le \delta \le +25$ ppm (Figure 4c,d), we observe the coexistence of two complexes in solution, each possessing average $C_{2v}$ symmetry on the NMR time scale. Because of the location of the H2 protons close to the paramagnetic center (Figure 4b), their large pseudocontact shifts can be exploited for probing speciation in solution with the detection of two singlets at a low magnetic field for Ln = Eu ($C_{Eu} = 4.0$; Figure 4c) and of two singlets at a high magnetic field for Ln = Pr ($C_{Pr} = -11.0$; Figure 4d). The existence of only two complexes in solution is thus confirmed for each complex, and their quantification can be obtained by the simple deconvolution and integration of the $^1$H NMR signals of H2.[10c,11,15]

**Thermodynamic Parameters for the Dimerization of [Ln(L*k*)$(NO_3)_3$] in $CD_2Cl_2$ (L*k* = L5−14 and Ln = Pr, Eu).** Despite the first mention of the dimerization process

**Scheme 2.** Synthesis of Compounds **1**−**3** [$^i$Prop = 2-Propanol and dppf = 1,1′-Bis(diphenylphosphino)ferrocene]

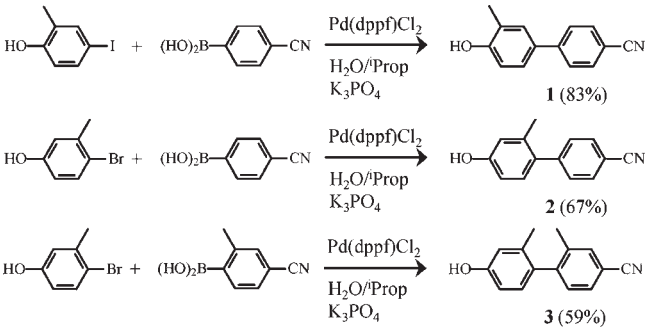


shown in equilibrium (1) already in 1992 when analyzing $^1$H−$^1$H COSY NMR spectra of simple nine-coordinate [(2,6-bis(*N*-methylbenzimidazol-2-yl)pyridine)Eu$(NO_3)_3$] complexes,[17] its unambiguous demonstration was delayed by more than a decade with the ultimate characterization of the polycatenar complexes [Eu(**L15$^{Cn}$**)$(NO_3)_3$] (bent shape, 5,5′-disubstituted) and [Eu(**L16$^{Cn}$**)$(NO_3)_3$] (rodlike shape, 6,6′-disubstituted) in solution (measurements of translational self-diffusion coefficients by DOSY NMR) and in the solid state (molecular structures obtained from X-ray diffraction data; Figure 5).[15] van't Hoff plots derived from analysis of the integration of variable-temperature $^1$H NMR (VT-NMR, $CD_2Cl_2$) data yielded $\Delta H^{\circ Eu,\mathbf{L15C12}}_{dim} = -54(4)$ kJ·mol$^{-1}$ and $\Delta S^{\circ Eu,\mathbf{L15C12}}_{dim} = -162(16)$ J·mol$^{-1}$·K$^{-1}$ for the dimerization [equilibrium (1)] operating between two bent polycatenar europium complexes, and $\Delta H^{\circ Eu,\mathbf{L16C12}}_{dim} = -25(2)$ kJ·mol$^{-1}$ and $\Delta S^{\circ Eu,\mathbf{L16C12}}_{dim} = -47(5)$ J·mol$^{-1}$·K$^{-1}$ for the same process applied to the rodlike analogous complexes (Figure 5).[15] Already noticed in 2005,[15] the parallel increase of $\Delta H^{Eu,\mathbf{Lk}}_{dim}$ and $\Delta S^{Eu,\mathbf{Lk}}_{dim}$ on going from [Eu(**L15$^{C12}$**)$(NO_3)_3$] to [Eu(**L16$^{C12}$**)$(NO_3)_3$] is reminiscent of the enthalpy/entropy compensation concept, which claims that any reduction of the intermolecular interactions responsible for the formation of the dimer ($\Delta H^{\circ Eu,\mathbf{Lk}}_{dim}$ becomes less negative) produces a change in dynamics between the two states measured by an increase of $\Delta S^{Eu,\mathbf{Lk}}_{dim}$.[18] Preliminary results showed that equilibrium (1) also holds for the dendrimeric complexes [Eu(**L5**)$(NO_3)_3$][10c] and [Eu(**L6**)$(NO_3)_3$],[11] for which measurement of the diffusion coefficients unambiguously demonstrated the coexistence around room temperature of the monomer and dimer in $CD_2Cl_2$ (Table 1).[10c,11]

The thorough recording of VT-NMR spectra for the 20 complexes [Ln(**Lk**)$(NO_3)_3$] (Ln = Pr, Eu; $k$ = 5−14) in $CD_2Cl_2$ in the 273−318 K range confirms this behavior and systematically shows the interconversion occurring between the monomer and dimer according to equilibrium (1). Moreover, at the concentration used for NMR measurements ($|\mathbf{Lk}|_{tot} \approx 10$ mM), the cumulative stability constants $\beta^{Ln,\mathbf{Lk}}_{1,1}$ and $\beta^{Ln,\mathbf{Lk}}_{2,2}$ are large enough to prevent

(16) (a) Golding, R. M.; Halton, M. P. *Aust. J. Chem.* **1972**, *25*, 2577–2581. (b) Pinkerton, A. A.; Rossier, M.; Spiliadis, S. *J. Magn. Reson.* **1985**, *64*, 420–425. (c) Bleaney, B. *J. Magn. Reson.* **1972**, *8*, 91–100. (d) For a tutorial review, see: Piguet, C.; Geraldes, C. F. G. C. In *Handbook on the Physics and Chemistry of Rare Earths*; Gschneidner, K. A., Jr., Bünzli, J.-C. G., Pecharsky, V. K., Eds.; Elsevier Science: Amsterdam, The Netherlands, 2003; Vol. *33*, pp 353−463.

(17) Piguet, C.; Williams, A. F.; Bernardinelli, G.; Moret, E.; Bünzli, J.-C. G. *Helv. Chim. Acta* **1992**, *75*, 1697–1717.

(18) (a) Searle, M. S.; Williams, D. H. *J. Am. Chem. Soc.* **1992**, *114*, 10690–10197. (b) Dunitz, J. D. *Chem. Biol.* **1995**, *2*, 709–712. (c) Searle, M. S.; Westwell, M. S.; Williams, D. H. *J. Chem. Soc., Perkin Trans. II* **1995**, 141–151. (d) Williams, D. H.; O'Brien, D. P.; Bardsley, B. *J. Am. Chem. Soc.* **2001**, *123*, 737–738. (e) Levchenko, A. A.; Yee, C. K.; Parikh, A. N.; Navrotsky, A. *Chem. Mater.* **2005**, *17*, 5428–5438.

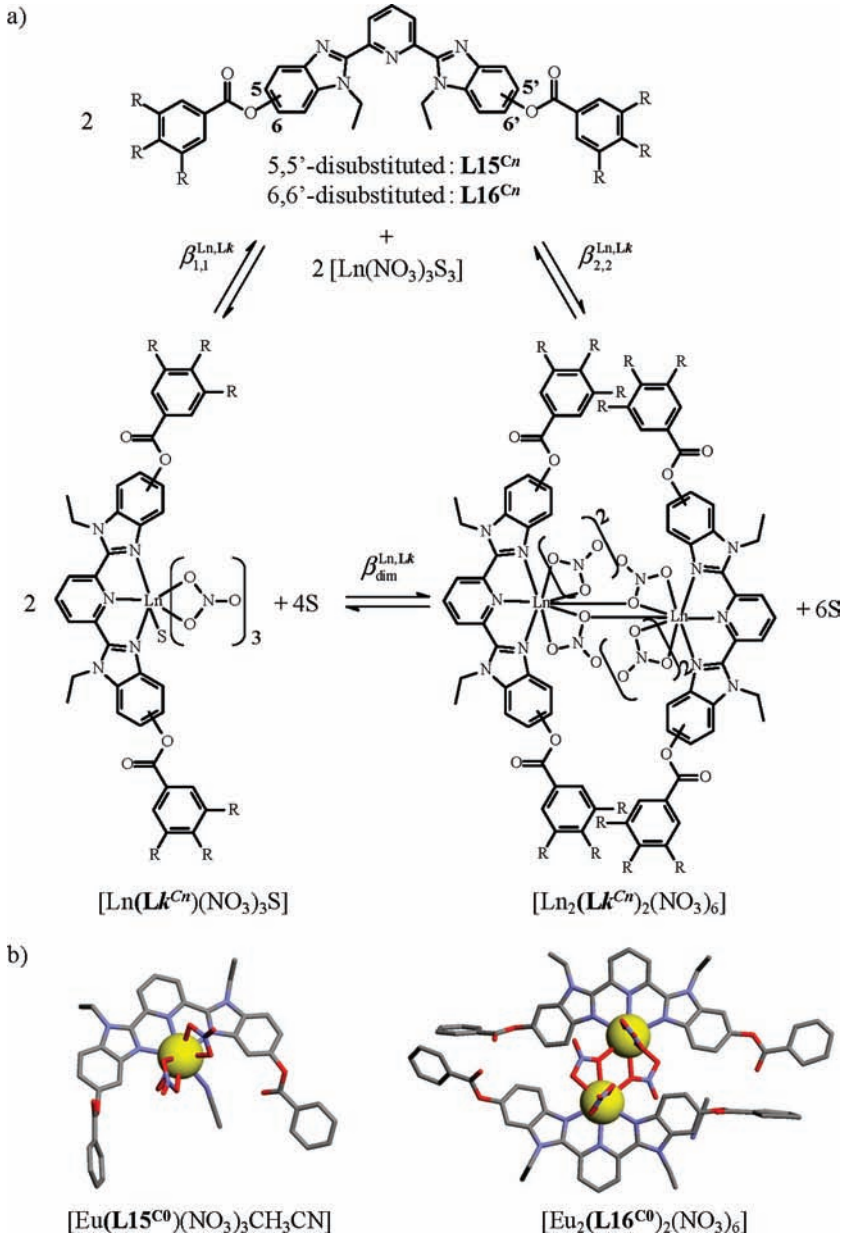


**Figure 5.** (a) Thermodynamic equilibria for the complexation of $\mathbf{L15}^{\mathbf{Cn}}$ or $\mathbf{L16}^{\mathbf{Cn}}$ with $Ln(NO_3)_3$ [R = H ($\mathbf{Lk}^{\mathbf{C0}}$), $OCH_3$ ($\mathbf{Lk}^{\mathbf{C1}}$), and $OC_{12}H_{25}$ ($\mathbf{Lk}^{\mathbf{C12}}$); S = solvent molecule] and (b) molecular structures of the monomeric $[Eu(\mathbf{L15}^{\mathbf{C0}})(NO_3)_3CH_3CN]$ and dimeric $[Eu_2(\mathbf{L16}^{\mathbf{C0}})_2(NO_3)_6]$ complexes determined by X-ray diffraction.[15].

detectable decomplexation. The speciation in solution required for extraction of the thermodynamic data for each system is thus obtained by the following procedure. (1) The signals of the paramagnetically shifted protons H2 in the monomer and dimer are located in the $^1$H NMR spectrum, and their relative intensities upon dilution are recorded (Figure 6a). Because of the law of mass action, the quantity of monomer increases upon dilution, which allows the unambiguous assignment of the signals for the monomer and dimer. (2) The VT-NMR spectra are recorded in $CD_2Cl_2$, and the intensity of each signal for H2 is obtained by deconvoluting the experimental trace with a single Lorentz function for each peak (Figures 6b and S1 in the Supporting Information). The separated integrated intensities are then converted into concentrations by using the mass balance modulated by the number of protons contributing to each signal. (3) The dimerization constants are calculated at each temperature $\beta_{\mathrm{dim}}^{\mathrm{Ln},\mathbf{Lk}} = (|\mathrm{dimer}|/|\mathrm{monomer}|^2)c^{\theta}$ by using the standard $c^{\theta} = 1$ M concentration as the reference state.[19] The building of van't Hoff plots (eq 2) eventually gives $\Delta H^{\circ}_{\mathrm{dim}}{}^{\mathrm{Ln},\mathbf{Lk}}$ and $\Delta S^{\circ}_{\mathrm{dim}}{}^{\mathrm{Ln},\mathbf{Lk}}$ as the slopes and intercepts, respectively, of the linear correlations (Figure 6c).

$$-R\ln(\beta_{\mathrm{dim}}^{\mathrm{Ln},\mathbf{Lk}}) = \frac{\Delta H^{\circ}_{\mathrm{dim}}{}^{\mathrm{Ln},\mathbf{Lk}}}{T} - \Delta S^{\circ}_{\mathrm{dim}}{}^{\mathrm{Ln},\mathbf{Lk}} \qquad (2)$$

For some complexes, severe overlap between the signals of H2 in the monomer and dimer may limit the precision of the van't Hoff analyses (Figure S2a in the Supporting

(19) (a) Martell, A. E. *Adv. Chem. Ser.* **1967**, *62*, 272–294. (b) Munro, D. *Chem. Brit.* **1977**, *13*, 100–105. (c) Simmons, E. L. *J. Chem. Educ.* **1979**, *56*, 578–579. (d) Chung, C.-S. *J. Chem. Educ.* **1984**, *61*, 1062–1064.

**Table 1.** Thermodynamic Parameters $\Delta H^{\circ Ln,Lk}_{dim}$, $\Delta S^{\circ Ln,Lk}_{dim}$, $\Delta G^{\circ Ln,Lk}_{dim}$, $\beta^{\circ Ln,Lk}_{dim}$, $T^{Ln,Lk}_{dim,50\%}$, and $T^{Lk}_{crit}$ for Equilibrium (I) for Ln = Pr and Eu and Ligands **L5**−**L14** ($CD_2Cl_2$)[a]

| | $\Delta H^{\circ Ln,Lk}_{dim}$ /kJ·mol$^{-1}$ | $\Delta S^{\circ Ln,Lk}_{dim}$ /J·mol$^{-1}$·K$^{-1}$ | $\Delta G^{\circ Ln,Lk}_{dim}$ /kJ·mol$^{-1}$ | $\beta^{\circ Ln,Lk}_{dim}$ [b] | $T^{Ln,Lk}_{dim,50\%}$ [c]/°C | $T^{Lk}_{crit}$ [d]/K |
|---|---|---|---|---|---|---|
| [Pr(**L5**)$(NO_3)_3$] | −26(4) | −43(15) | −12.9(3) | 183(21) | 43(7) | 236 |
| [Eu(**L5**)$(NO_3)_3$] | −55(4) | −166(11) | −5.5[e] | 9[e] | −4[e] | |
| [Pr(**L6**)$(NO_3)_3$] | −33(4) | −72(14) | −11.9(2) | 121(11) | 29(3) | 572 |
| [Eu(**L6**)$(NO_3)_3$] | −25(1) | −58(5) | −7.93(5) | 24.6(5) | −11(2) | |
| [Pr(**L7**)$(NO_3)_3$] | −7.7(6) | 15(2) | −12.06(3) | 130(2) | 52(3) | 208 |
| [Eu(**L7**)$(NO_3)_3$] | −17.9(8) | −34(3) | −7.82(3) | 23.5(3) | −25(2) | |
| [Pr(**L8**)$(NO_3)_3$] | −2.8(8) | 31(3) | −11.92(4) | 123(2) | 92(26) | 280 |
| [Eu(**L8**)$(NO_3)_3$] | −31.9(5) | −73(2) | −10.01(3) | 56.8(6) | 12.3(3) | |
| [Pr(**L9**)$(NO_3)_3$] | *f* | *f* | *f* | *f* | *f* | *f* |
| [Eu(**L9**)$(NO_3)_3$] | 2(6) | 40(20) | −9.93(6) | 55(4) | 770(755) | |
| [Pr(**L10**)$(NO_3)_3$] | −5.2(8) | 23(3) | −12.01(4) | 128(2) | 64(8) | 268 |
| [Eu(**L10**)$(NO_3)_3$] | −23.4(8) | −45(5) | −10.03(3) | 57.2(7) | 8.2(8) | |
| [Pr(**L11**)$(NO_3)_3$] | −35(8) | −50(27) | −20.3(8) | 3525(435) | 126(30) | 809 |
| [Eu(**L11**)$(NO_3)_3$] | −18(2) | −29(6) | −8.83(6) | 35.3(9) | −13(4) | |
| [Pr(**L12**)$(NO_3)_3$] | −43(4) | −91(15) | −15.3(2) | 487(31) | 55(3) | 545 |
| [Eu(**L12**)$(NO_3)_3$] | −25(3) | −58(9) | −7.3(1) | 18.9(8) | −18(5) | |
| [Pr(**L13**)$(NO_3)_3$][c] | *f* | *f* | *f* | *f* | *f* | *f* |
| [Eu(**L13**)$(NO_3)_3$] | −25(5) | −60(17) | −7.1(2) | 17(1) | −19(9) | |
| [Pr(**L14**)$(NO_3)_3$] | −62(5) | −148(15) | −17.7(2) | 1254(83) | 59(3) | 375 |
| [Eu(**L14**)$(NO_3)_3$] | −17(2) | −28(6) | −8.69(6) | 33.3(9) | −16(4) | |

[a] The standard deviations for $\Delta H^{\circ Ln,Lk}_{dim}$ and $\Delta S^{\circ Ln,Lk}_{dim}$ were obtained from the linear least-squares fits, while those for $\Delta G^{\circ Ln,Lk}_{dim}$, $\beta^{\circ Ln,Lk}_{dim}$, and $T^{Ln,Lk}_{dim,50\%}$ were computed by taking into account the interdependence of $\Delta H^{\circ Ln,Lk}_{dim}$ and $\Delta S^{\circ Ln,Lk}_{dim}$ given by the covariance matrices.[21] [b] The dimerization constant was calculated at 298 K by using the standard 1 M concentration as the reference state. [c] $T^{Ln,Lk}_{dim,50\%} = \Delta H^{\circ Ln,Lk}_{dim}/(\Delta S^{\circ Ln,Lk}_{dim} + R \ln C^{Lk}_{tot})$ is the temperature at which the monomer represents 50% of the ligand distribution in solution (calculated with a total ligand concentration of $C^{Lk}_{tot} = 0.01$ M used for NMR measurements; see Appendix 1 in the Supporting Information). [d] Critical temperature $T^{Lk}_{crit} = (\Delta H^{\circ Eu,Lk}_{dim} - \Delta H^{\circ Pr,Lk}_{dim})/\Delta S^{\circ Eu,Lk}_{dim} - \Delta H^{\circ Pr,Lk}_{dim}$ for which $\Delta G^{Pr,Lk}_{dim} = \Delta G^{Eu,Lk}_{dim}$ (estimated for the centroids of enthalpic and entropic contributions). [e] Taken from ref 10b. [f] Spectral overlap prevents analysis of the VT-NMR spectra.

Information) or even prevents the estimation of the thermodynamic parameters (Figure S2b in the Supporting Information). The experimental data $\Delta H^{\circ Ln,Lk}_{dim}$ and $\Delta S^{\circ Ln,Lk}_{dim}$ obtained for the 18 accessible complexes are collected in Table 1.

Plots of $\Delta H^{\circ Ln,Lk}_{dim}$ versus $\Delta S^{\circ Ln,Lk}_{dim}$ show two remarkably linear relationships given by eqs 3 and 4 including all ligands interacting with either Ln = Pr (eq 3 and Figure 7a) or Ln = Eu (eq 4 and Figure 7b).

$$\Delta H^{\circ Pr,Lk}_{dim} = 329(17)\Delta S^{\circ Pr,Lk}_{dim} - 13054(1203)\ \text{J·mol}^{-1} \quad (3)$$

$$\Delta H^{\circ Eu,Lk}_{dim} = 278(7)\Delta S^{\circ Eu,Lk}_{dim} - 9428(524)\ \text{J·mol}^{-1} \quad (4)$$

Relationships like eqs 3 and 4 are often referred to as extrathermodynamic because of their lack of basis in the laws of thermodynamics.[20] The positive correlation found between $\Delta H^{\circ Ln,Lk}_{dim}$ and $\Delta S^{\circ Ln,Lk}_{dim}$ is referred to as compensation because it tends to minimize changes in $\Delta G^{\circ Ln,Lk}_{dim}$ across the series.[18] The slope of each correlation has Kelvin units and is called the compensation temperature, $T^{Ln}_{comp}$.[22] At this temperature, any variation in the standard enthalpy of dimerization, $\Delta H^{\circ Ln,Lk}_{dim}$, across the series is balanced by an exact compensating variation in the standard entropy, $T^{Ln}_{comp}\Delta S^{\circ Ln,Lk}_{dim}$, thus leading to processes displaying the same exergonicities, which are given by the intercepts of the linear correlations $(\Delta G^{Pr}_{dim}(T^{Pr}_{comp} = 329\ \text{K}) = -13.0(1.2)\ \text{kJ·mol}^{-1}$ and $(\Delta G^{Eu}_{dim}(T^{Eu}_{comp} = 278\ \text{K}) = -9.4(5)\ \text{kJ·mol}^{-1})$. Because (i) $(\Delta G^{Pr}_{dim}(T^{Pr}_{comp} = 329\ \text{K}) < (\Delta G^{Eu}_{dim}(T^{Eu}_{comp} = 278\ \text{K})$ and (ii) the computed critical temperature $T^{Lk}_{crit}$ at which $\Delta G^{Pr,Lk}_{dim} = \Delta G^{Eu,Lk}_{dim}$ is outside the 280−329 K temperature range, we can deduce that $\Delta G^{\circ Pr,Lk}_{dim} < \Delta G^{\circ Eu,Lk}_{dim}$ around room temperature, so the dimerization process is systematically more favorable for the larger praseodymium cation in $CD_2Cl_2$ (Table 1, column 5). However, prior to further interpretation of the observed correlations between the enthalpic and entropic parameters across this series of ligands, it is worth stressing here that such apparent compensations seen for several physical or chemical intermolecular associations may result from a statistical artifact linked to the van't Hoff analyses, which do not independently measure $\Delta H$ and $\Delta S$.[23−25] Moreover, the narrow experimental temperature range used, which is required for reasonably considering temperature-independent values for $\Delta H$ and $\Delta S$, also limits the precision of the separation of enthalpic and entropic contributions. Beyond the systematic calculations of the covariance matrix[21] for each van't Hoff plot, which indeed display high values, but significantly smaller than 1.0, Krug and co-workers proposed several additional tests that can be applied to evaluate the possible significance of apparent enthalpy/entropy correlations.[24] First, the observed compensation temperature $T^{Ln}_{comp}$ must be

(20) Starikov, E. B.; Norden, B. *J. Phys. Chem. B* **2007**, *111*, 14431–14435.
(21) For each least-squares fit analysis, we used the macro *LS1* for computing the covariance matrix and the macro *Propagation* for estimating the standard deviations. De Levie, R. *Advanced Excel for Scientific Data Analysis*, 2nd ed.; Oxford University Press: Oxford, U.K., 2008.
(22) Leffler, J. E. *J. Org. Chem.* **1955**, *20*, 1202–1231.
(23) (a) Liu, L.; Guo, Q. X. *Chem. Rev.* **2001**, *101*, 673–695. (b) Sharp, K. *Protein Sci.* **2001**, *10*, 661–667.
(24) (a) Krug, R. R.; Hunter, W. G.; Grieger, R. A. *J. Phys. Chem.* **1976**, *80*, 2335–2341. (b) Krug, R. R.; Hunter, W. R.; Grieger, R. A. *J. Phys. Chem.* **1976**, *80*, 2341–2351. (c) Krug, R. R.; Hunter, W. G.; Grieger, R. A. *Nature* **1976**, *261*, 566–567. (d) Linert, W.; Jameson, R. F. *Chem. Soc. Rev.* **1989**, *18*, 477–505.
(25) Leung, D. H.; Bergman, R. G.; Raymond, K. N. *J. Am. Chem. Soc.* **2008**, *130*, 2798–2805.

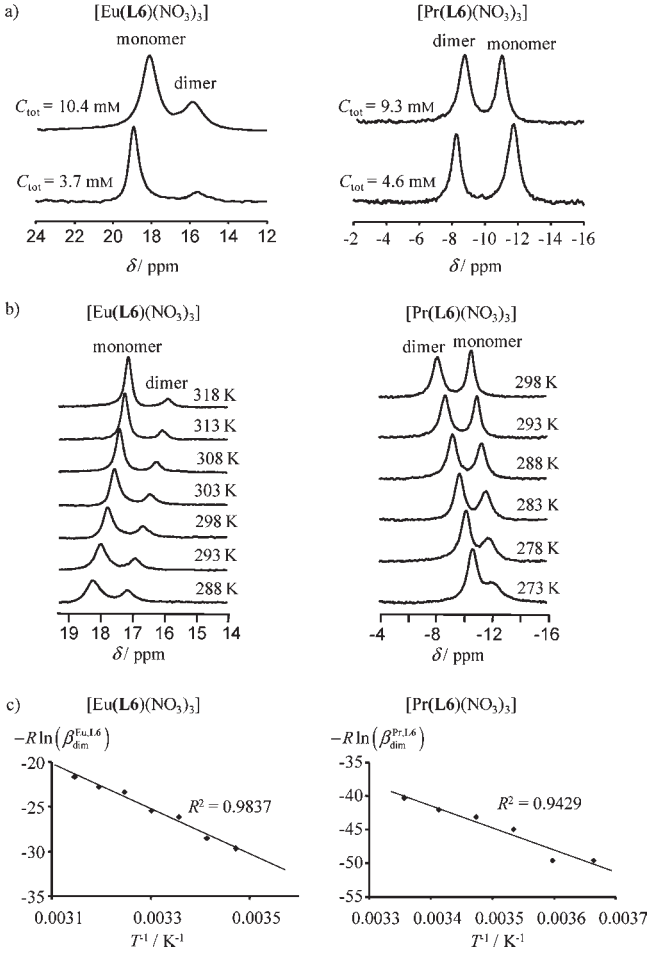


**Figure 6.** Experimental determination of thermodynamic enthalpic $\Delta H_{dim}^{Ln,Lk}$ and entropic $\Delta S_{dim}^{Ln,Lk}$ contributions to equilibrium (1) by exploiting the VT-NMR spectra recorded for [Ln(**L6**)$(NO_3)_3$] (Ln = Pr, Eu; $CD_2Cl_2$): (a) concentration and (b) temperature dependences of the intensity of the signals of proton H2 in the monomer and dimer; (c) associated van't Hoff plots ($R^2$ = coefficient of determination).

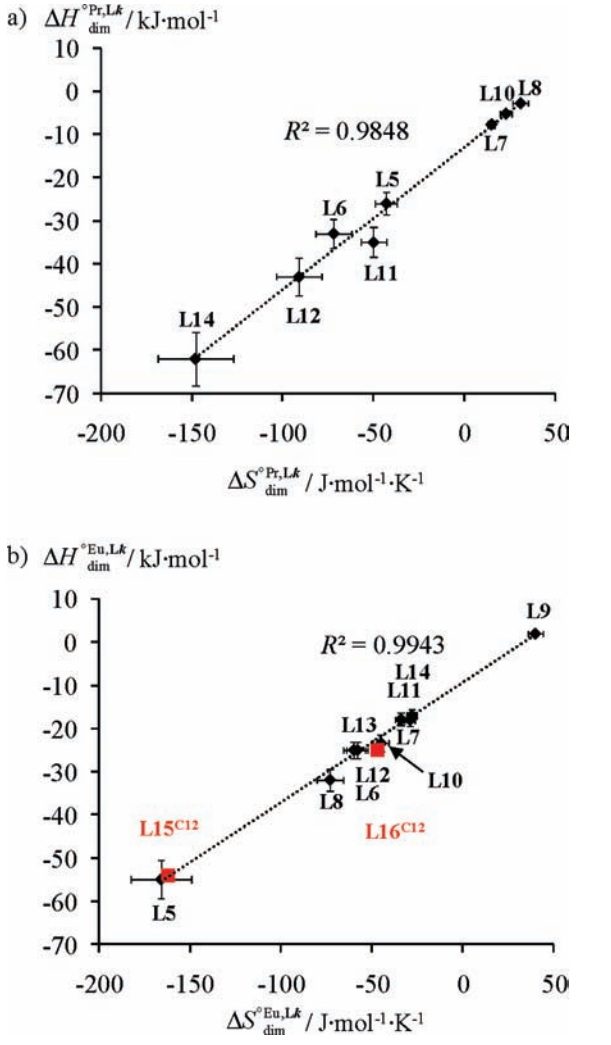


**Figure 7.** Plots of enthalpy versus entropy values for the dimerization process shown in equilibrium (1) and occurring in $CD_2Cl_2$ for (a) [Pr(**L*k***)$(NO_3)_3$] (**L*k*** = **L5**−**L14** except **L9** and **L13**; see Table 1) and (b) [Eu(**L*k***)$(NO_3)_3$] (**L*k*** = **L5**−**L14**; $R^2$ = coefficient of determination). The red points correspond to those previously reported for [Eu(**L15**$^{C12}$)$(NO_3)_3$] and [Eu(**L16**$^{C12}$)$(NO_3)_3$].[15]

significantly different from the average experimental temperature $T_{exp}^{Ln}$. For Ln = Pr, $T_{comp}^{Pr}$ = 329 K can be compared with $T_{exp}^{Pr}$ = 285 K, while for Ln = Eu, we obtain $T_{comp}^{Eu}$ = 278 K and $T_{exp}^{Eu}$ = 303 K (Figure 6). The two absolute gaps $\Delta T^{Pr} = |T_{comp}^{Pr} - T_{exp}^{Pr}| = 44$ K and $\Delta T^{Eu} = |T_{comp}^{Eu} - T_{exp}^{Eu}| = 25$ K are significantly larger than the uncertainties affecting $T_{comp}^{Ln}$ (eqs 3 and 4) and are of magnitude comparable to those found by Raymond, Bergman, and co-workers for significant enthalpy/entropy compensation controlling host−guest encapsulations.[25] Surprisingly, these authors suggest a second test, which claims that, when plotted together, the van't Hoff correlations $-R\ln(\beta_{dim}^{Ln,Lk})$ versus $T^{-1}$ for a set of related reactions should intersect at a common temperature.[25] However, this second criterion is a consequence of the linearity of eqs 3 and 4, because all reactions considered within a linear series display the same ergonicity at $T_{comp}^{Ln}$ and thus produce identical stability constants $\beta_{dim}^{Ln,Lk}$ at this temperature. Figure S3 (Supporting Information) shows collections of the van't Hoff plots for Ln = Pr and Eu across the ligand series, which obviously confirm this statement. The larger deviation found for [Pr(**L11**)$(NO_3)_3$] (Figure S3a in the Supporting Information) can be easily predicted when considering the enthalpy/entropy plots of Figure 7a, whereby this complex displays the larger deviation from the linear trendline. Because the three above-mentioned criteria are obeyed, we conclude that the observed correlations between enthalpic and entropic values for the dimerization of [Ln(**L*k***)$(NO_3)_3$] in $CD_2Cl_2$ have true chemical significance for Ln = Pr and Eu across the complete ligand series. A close scrutiny at the linear enthalpy/entropy compensations shown in Figure 7 does not reveal any clear trend associated with either methyl substitution, the nature of the ligand backbone, or the molecular weights of the complexes. Interestingly, consideration of the $\langle \Delta S_{dim}^{\circ Eu,L15C12}, \Delta H_{dim}^{\circ Eu,L15C12} \rangle \langle \Delta S_{dim}^{\circ Eu,L16C12}, \Delta H_{dim}^{\circ Eu,L16C12} \rangle$ pairs reported for the polycatenar complexes matches the linear correlation for Ln = Eu (red points in Figure 7b), which further supports the minor effects of the primary ligand structure on the compensating trend. However, the existence of two different series for Ln = Pr and Eu indicates that the minor change in the ionic radius has a global impact on dimerization, leading to [$Ln_2$(**L*k***)$_2$-$(NO_3)_6$], a behavior that can be tentatively assigned to the preference of the larger cation for 10-coordination in the

nitrato-bridged dimer (Figure 5).[15] Following the classical thermodynamic desolvation/association mechanism,[26] each complexation process can be then separated into two successive equilibria (5) and (6) displaying opposite enthalpic and entropic contributions (S = solvent molecule).[26]

$$2[\mathrm{Ln}(\mathbf{L}\boldsymbol{k})(\mathrm{NO_3})_3(\mathrm{S})_n] \rightleftharpoons 2[\mathrm{Ln}(\mathbf{L}\boldsymbol{k})(\mathrm{NO_3})_3(\mathrm{S})_{n-p}] + 2p\mathrm{S}$$
$$\Delta G^{\mathrm{Ln},\mathbf{L}\boldsymbol{k}}_{\mathrm{desolv}} = \Delta H^{\mathrm{Ln},\mathbf{L}\boldsymbol{k}}_{\mathrm{desolv}} - T\Delta S^{\mathrm{Ln},\mathbf{L}\boldsymbol{k}}_{\mathrm{desolv}} \quad (5)$$

$$2[\mathrm{Ln}(\mathbf{L}\boldsymbol{k})(\mathrm{NO_3})_3(\mathrm{S})_{n-p}] \rightleftharpoons [\mathrm{Ln_2}(\mathbf{L}\boldsymbol{k})_2(\mathrm{NO_3})_6(\mathrm{S})_{2(n-p)}]$$
$$\Delta G^{\mathrm{Ln},\mathbf{L}\boldsymbol{k}}_{\mathrm{ass.}} = \Delta H^{\mathrm{Ln},\mathbf{L}\boldsymbol{k}}_{\mathrm{ass.}} - T\Delta S^{\mathrm{Ln},\mathbf{L}\boldsymbol{k}}_{\mathrm{ass.}} \quad (6)$$

In the weakly polar $CD_2Cl_2$ solvent, the desolvation step (eq 5) can be reasonably assumed to be similar within a series of complexes of similar molecular weight, differing only by peripheral methyl substitutions (family 1, **L5** and **L6**; family 2, **L7**−**L10**; family 3, **L11**−**L14**). Consequently, within each family, variation of $\Delta G^{\mathrm{Ln},\mathbf{L}\boldsymbol{k}}_{\mathrm{dim}} = \Delta G^{\mathrm{Ln},\mathbf{L}\boldsymbol{k}}_{\mathrm{desolv}} + \Delta G^{\mathrm{Ln},\mathbf{L}\boldsymbol{k}}_{\mathrm{ass.}}$ essentially reflects changes in $\Delta G^{\mathrm{Ln},\mathbf{L}\boldsymbol{k}}_{\mathrm{ass.}}$. Because lanthanide−ligand bonds are mainly electrostatic, the association process shown in eq 6 can be approached by a simple (nonquantum) model catching the physical forces of interest responsible for the formation of a dimer from two molecules of monomer.[27] As demonstrated by Ford,[27b] the enthalpic and entropic components of such an association process are given by eqs 7 and 8, respectively ($u_{\min}$ is the minimum of the binding potential, $k_b$ is Boltzmann's constant, $\kappa$ is the force constant of the interaction, and $c^\theta = 1/V^\theta$ is the concentration of the reference state).

$$\Delta H_{\mathrm{ass.}} = u_{\min} + \frac{3}{2}k_bT \quad (7)$$

$$\Delta S_{\mathrm{ass.}} = k_b \ln\left(\frac{(2\pi e)^{3/2}}{V^\theta}\right) - \frac{3}{2}k_b \ln\left(\frac{\kappa}{k_bT}\right) \quad (8)$$

According to eqs 7 and 8, the enthalpy/entropy compensation (i.e., a positive correlation) in $\Delta G^{\mathrm{Ln},\mathbf{L}\boldsymbol{k}}_{\mathrm{ass.}}$ implies that $u_{\min}$ and $\kappa$ move in opposite directions, so that $\Delta H^{\mathrm{Ln},\mathbf{L}\boldsymbol{k}}_{\mathrm{ass.}}$ and $\Delta S^{\mathrm{Ln},\mathbf{L}\boldsymbol{k}}_{\mathrm{ass.}}$ both decrease and increase, respectively.[27b] Following this simple reasoning, the intermolecular dimerization shown in equilibrium (6) can be modeled with a simple Lennard-Jones (12,6) potential $V = 4\varepsilon\{(r_0/r)^{12} - (r_0/r)^6\}$, which only resorts to two parameters: (i) the minimum of the attractive well depth $\varepsilon$ and (ii) the intermolecular separation $r_0$ at which the potential of the interaction is zero [$V(r_0) = 0$; Figure 8]. While the correlation between the well depth and the binding potential is trivial, $u_{\min} = -\varepsilon$ ($u_{\min} < 0$), an analytical formulation for the force constant requires application of the harmonic approximation (eq 9), from which we can write $\kappa(r_0 - 2^{1/6}r_0)^2/2 = \varepsilon$ . A straightforward algebric transformation

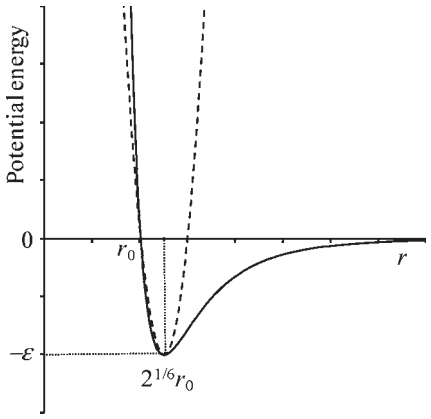


**Figure 8.** Representation of a Lennard-Jones (12,6) potential (full trace) with interpretation of the $\varepsilon$ and $r_0$ parameters and its harmonic approximation (eq 9, dashed trace) modeling the intermolecular interactions responsible for the formation of the dimer $[\mathrm{Ln_2}(\mathbf{L}\boldsymbol{k})_2(\mathrm{NO_3})_6]$.

eventually gives $\kappa = [2/(1 - 2^{1/6})^2]\varepsilon/(r_0)^2$ ($\kappa > 0$; see Appendix 2 in the Supporting Information).

$$V_{\mathrm{harm}}(r) = \frac{\varepsilon}{\alpha}[-2^{-7/6}(r/r_0)^2 + (r/r_0) + 2^{-7/6} - 1]$$
$$\text{with } \alpha = 1 - 2^{1/6} + 2^{-5/6} - 2^{-7/6} \quad (9)$$

Introducing the expression found for $u_{\min}$ and $\kappa$ into eqs 7 and 8, respectively, shows that the observed enthalpy/entropy compensation within a series occurs when $\varepsilon$ varies and $r_0$ is fixed. Consequently, within a family of ligands, the trend in the association process leading to $[\mathrm{Ln_2}(\mathbf{L}\boldsymbol{k})_2(\mathrm{NO_3})_6]$ can be thought of as an intermolecular cohesion, for which the magnitude of the interaction ($\Delta H^{\mathrm{Ln},\mathbf{L}\boldsymbol{k}}_{\mathrm{ass.}}$) is modulated by the peripheral methyl substitution, but the optimum intermolecular separation is fixed by the choice of the metal, which consequently provides entropic compensation due to changes in the dynamics between the two states (i.e., two monomers versus one dimer; Figure 8). In simple chemical words, we can say that the transformation of two monomers $[\mathrm{Ln}(\mathbf{L}\boldsymbol{k})(\mathrm{NO_3})_3]$ into the dimer $[\mathrm{Ln_2}(\mathbf{L}\boldsymbol{k})_2(\mathrm{NO_3})_6]$ relies on a primary interaction that depends on the size of the trivalent cation, which fixes the average intermolecular separation $r_0$ in our simple harmonic model. For a given metallic center, additional nonspecific interstrand interactions modulate $\Delta G^{\mathrm{Ln},\mathbf{L}\boldsymbol{k}}_{\mathrm{dim}}$ within the frame of enthalpy/entropy compensation. According to the molecular structures established for $[\mathrm{Eu}(\mathbf{L15^{C0}})(\mathrm{NO_3})_3(\mathrm{CH_3CN})]$, $[\mathrm{Lu}(\mathbf{L16^{C0}})(\mathrm{NO_3})_3]$, and $[\mathrm{Eu_2}(\mathbf{L16^{C0}})_2(\mathrm{NO_3})_6]$ (Figure 5),[15] we assign the primary interaction fixing $r_0$ to the formation of nitrate bridges between the metallic parts of the complexes, a process expected to be favored for the larger cation $Pr^{III}$, for which 10-coordination is easily adopted. The additional modulation of $\Delta H^{\mathrm{Ln},\mathbf{L}\boldsymbol{k}}_{\mathrm{dim}}$ and $\Delta S^{\mathrm{Ln},\mathbf{L}\boldsymbol{k}}_{\mathrm{dim}}$ within the frame of strict enthalpy/entropy compensation for each metal results from nondirectional van der Waals interactions between the polarizable parts of the semidendrimeric ligand strands. Increasing length (family 3 → family 2 → family 1), varying branching (family 1 vs family 2), or specific methyl substitution of the terminal cyanobiphenyl groups does influence the organization of the ligand strands and their interactions in the dimer, but we cannot

(26) (a) Choppin, G. R. *Lanthanide Probes in Life, Chemical and Earth Sciences*; Elsevier: Amsterdam, The Netherlands, 1989; Chapter 1. (b) Piguet, C.; Bünzli, J.-C. G. *Chem. Soc. Rev.* **1999**, *28*, 347–358.

(27) (a) Luo, H. B.; Sharp, K. *Proc. Natl. Acad. Sci. U.S.A.* **2002**, *99*, 10399–10404. (b) Ford, D. M. *J. Am. Chem. Soc.* **2005**, *127*, 16167–16170.

**Table 2.** Phase-Transition Temperatures and Enthalpy and Entropy Changes for Ligands **L5**−**L14**

| compound | transition[a] | $T$/°C | $\Delta H$ /kJ·mol$^{-1}$ | $\Delta S$ /J·mol$^{-1}$·K$^{-1}$ |
|---|---|---|---|---|
| **L5** | g → N | 52 | | |
| | N → I | 238 | 11.0 | 21.5 |
| **L6** | g → N | 50−70[b] | | |
| | N → I | 197 | 9.7 | 20.5 |
| **L7** | g → I | 118 | | |
| **L8** | g → I | 90 | | |
| **L9** | g → I | 85 | | |
| **L10** | g → I | 84 | | |
| **L11** | g → N | 70−80[b] | | |
| | N → I | 324[b] | | |
| **L12** | g → N | 70−80[b] | | |
| | N → I | 265[b] | | |
| **L13** | g → N | 70−80[b] | | |
| | N → I | 260[b] | | |
| **L14** | g → N | 70−80[b] | | |
| | N → I | 205[b] | | |

[a] g = glass, N = nematic phase, and I = isotropic fluid. Temperatures are given as the onset of the peak observed during the second heating processes. [b] The liquid-crystalline phases were identified from their optical textures and from SA-XRD studies.

detect trivial correlations between the chemical structures and the thermodynamic parameters of the interaction.

**Thermal and Liquid-Crystalline Properties of the Ligands L5−L14 and of Their Complexes [Ln(L*k*)(NO$_3$)$_3$].** The thermal behaviors of the ligands **L5**−**L14** (Table 2) and of their complexes (Table 3) have been investigated by a combination of thermogravimetric analysis (TGA), differential scanning calorimetry (DSC), polarized optical microscopy (POM), and small-angle X-ray diffraction (SA-XRD). First, the TGA traces systematically show the release of interstitial cocrystallized water molecules during the first heating process in the temperature range 80−140 °C. At higher temperature, decomposition of the free ligand starts around 350 °C, while the nitrato complexes [Ln(L*k*)(NO$_3$)$_3$] rapidly decompose upon entering the isotropic liquid phase around 180−200 °C (Tables 2 and 3 and Figure S4 in the Supporting Information). Therefore, the thermal behaviors are systematically discussed for the second heating/cooling cycle following an initial 25−100−25 °C cycle, which ensures the removal of all cocrystallized water molecules in the samples.

For ligands **L5**, **L6**, and **L11**−**L14**, for which the terminal cyanobiphenyl groups are connected to a linear 1-4 phenyl spacer (Figure 3), typical Schlieren textures are observed by POM in agreement with the formation of nematic mesophases (Table 2 and Figure S5 in the Supporting Information). The temperature of the N → I phase transition (Figure S6 in the Supporting Information) systematically decreases with the connections of an increasing number of methyl groups onto the terminal cyanobiphenyl units [$T_c$(**L5**) > $T_c$(**L6**) and $T_c$(**L11**) > $T_c$(**L12**) ≈ $T_c$(**L13**) > $T_c$(**L14**)]. This behavior suggests some reduction of the residual intermolecular cohesion in the nematic phases resulting from some limitation of the $\pi$ overlaps between methyl-substituted cyanobiphenyl groups ($\Delta H_c$ indeed decreases by 13% on going from **L5** to **L6**). In line with the previous detection of enthalpy/entropy compensation for the nondirectional association between the ligand strands of the dimeric complexes in a noncoordinating solvent, this reduction of $\Delta H_c$ is accompanied by a concomitant reduction in $\Delta S_c$ at the N → I phase transition (Table 2, entries 2 and 3). In order to gain further insight into the residual interstrand interactions responsible for the formation of the nematic phase, SA-XRD data have been collected in the mesophase of **L6** at 150 °C upon alignment of the sample in a magnetic field (1 T; Figure S7 in the Supporting Information). Beyond the standard diffuse reflection observed at ≈4.5 Å and assigned to the average separation between the molten alkyl chains of the rodlike ligands, an additional orthogonal diffuse band is detected at $d \approx 17$ Å, which is attributed to some nonspecific residual intermolecular interactions between the aromatic segments responsible for the global alignment along the director $\vec{n}$ (Figure 9a). Such observations in thermotropic nematic phases obtained by phase transitions from either lamellar crystalline or liquid-crystalline phases are very common; they generally correspond to the existence of residual cybotactic groups.[28] Because **L6** contains four flexible interaromatic segments

**Table 3.** Phase-Transition Temperatures and Enthalpy and Entropy Changes for Complexes [Ln(L*k*)(NO$_3$)$_3$] (L*k* = **L5**−**L14**)

| compound | transition[a] | $T$/°C | $\Delta H$ / kJ·mol$^{-1}$ | $\Delta S$ / J·mol$^{-1}$·K$^{-1}$ |
|---|---|---|---|---|
| [Lu(**L5**)(NO$_3$)$_3$] | g → SmA2 | 100[c] | | |
| | SmA2 → PCr [b] | 150[c] | | |
| | PCr → SmA2 | 170[c] | | |
| | SmA2 → I/Dec | 200 | 3.3 | 6.9 |
| [Tb(**L5**)(NO$_3$)$_3$] | g → SmA2 | 90[c] | | |
| | SmA2 → I/Dec | 190 | 15.0 | 32.3 |
| [Gd(**L5**)(NO$_3$)$_3$] | g → SmA2 | 85[c] | | |
| | SmA2 → I/Dec | 1880 | 9.1 | 19.8 |
| [Eu(**L5**)(NO$_3$)$_3$] | g → SmA2 | 80[c] | | |
| | SmA2 → I/Dec | 186 | 11.1 | 24.2 |
| [Pr(**L5**)(NO$_3$)$_3$] | g → SmA2 | 80[c] | | |
| | SmA2 → Dec | 190[c] | | −3 |
| [Lu(**L6**)(NO$_3$)$_3$] | g → L | 90−100[c] | | |
| | L → N | 130 | 0.8 | 1.9 |
| | N → I/Dec | 144 | 6.9 | 16.4 |
| [Y(**L6**)(NO$_3$)$_3$] | g → SmA2 | 90−110[c] | | |
| | SmA2 → N | 134 | 1.5 | 3.7 |
| | N → I/Dec | 144 | 4.5 | 10.7 |
| [Tb(**L6**)(NO$_3$)$_3$] | g → SmA2 | 90−100[c] | | |
| | SmA2 → SmAd | 137 | 2.8 | 6.9 |
| | SmAd → I/Dec | 144 | 1.9 | 4.5 |
| [Gd(**L6**)(NO$_3$)$_3$] | g → SmA2 | 90−110[c] | | |
| | SmA2 → SmAd | 139 | 2.3 | 5.5 |
| | SmAd → I/Dec | 144 | 3.4 | 8.2 |
| [Eu(**L6**)(NO$_3$)$_3$] | g → SmA2 | 90−110[c] | | |
| | SmA2 → N | 138 | 2.4 | 5.8 |
| | N → I | 144 | 4.9 | 11.8 |
| [Pr(**L6**)(NO$_3$)$_3$] | g → SmA2 | 90−110[c] | | |
| | SmA2 → I | 147 | 17.0 | 40.4 |
| [La(**L6**)(NO$_3$)$_3$] | g → SmA2 | 90−110[c] | | |
| | SmA2 → I | 159 | 18.5 | 42.8 |
| [Ln(L*k*)(NO$_3$)$_3$] [d] | g → I | 110−120[c] | | |
| [Ln(L*k*)(NO$_3$)$_3$] [e] | g → I/Dec | 180−200[c] | | |

[a] g = glass and L = lamellar phase shown in Figure 9b, SmA2 = bilayer smectic A phase, SmAd = partially interdigitated smectic A phase, N = nematic phase, I = isotropic fluid, and Dec = decomposition. Temperatures are given as the onset of the peak observed during the second heating processes. [b] Re-entrant partially crystallized phase (PCr). [c] The liquid-crystalline phases were identified from their optical textures and/or from SA-XRD studies. [d] Ln = La, Pr, Eu, and Lu and L*k* = **L7**−**L10**. [e] Ln = La, Pr, Eu, and Lu and L*k* = **L11**−**L14**.

(28) Mamlouk, H.; Heinrich, B.; Bourgogne, C.; Donnio, B.; Guillon, D.; Felder-Flesch, D. *J. Mater. Chem.* **2007**, *17*, 2199–2205.

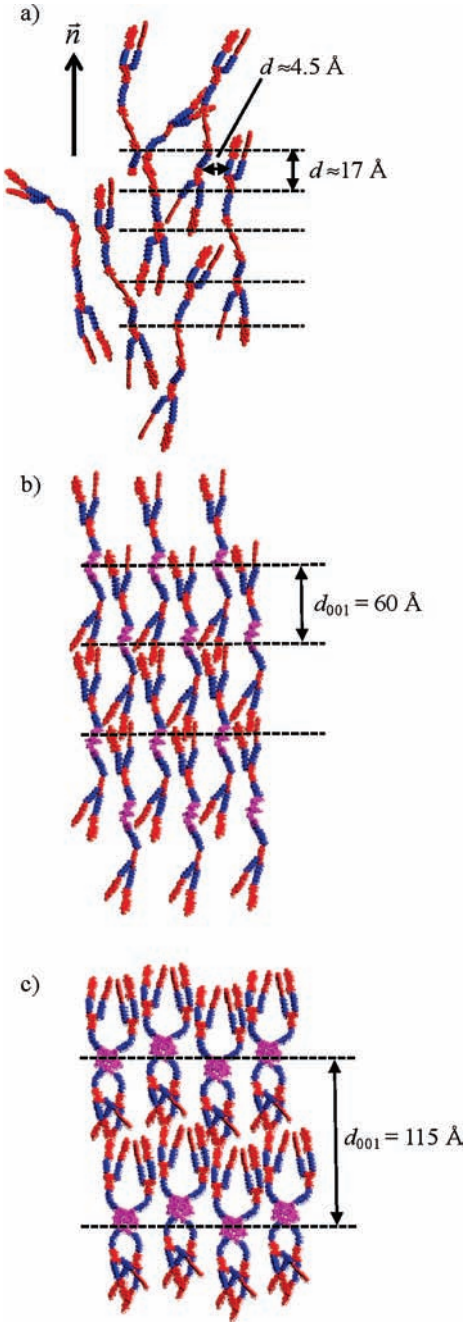


**Figure 9.** Proposed organizations in (a) the nematic phase of **L6**, (b) the layered mesophase of [Lu(**L6**)$(NO_3)_3$], and (c) the SmA2 phase of [Ln(**L6**)$(NO_3)_3$] (Ln = La, Pr, Eu) as deduced from POM and SA-XRD data. Color code: red, aromatic groups; blue, aliphatic chains; violet, coordinated benzimidazole−pyridine−benzimidazole units.

regularly spaced along the strand, we can estimate an average total length of $4 \times 17 \approx 68$ Å for the ligand in the nematic mesophase, which is much shorter than ca. 119 Å estimated by molecular modeling of **L5** or **L6** in their extended form (Figure 9a).[10b,11] This discrepancy can be reasonably assigned to the combination of (i) the shrinking of the flexible alkyl segments for fitting the large molecular area fixed by the rigid aromatic rods of the ligand and (ii) the fluctuation of the alignment of the mesogens along the director in the nematic phase.[28] The direct connection of the cyanobiphenyl groups to the divergent 1,3-phenyl spacer in ligands **L7**−**L10** removes the formation of nematic phases, and the DSC trace shows a vitrous transition around 90−120 °C (Figure S8, in the Supporting Information), leading to the disappearance of any specific texture by POM. The associated SA-XRD profiles do not exhibit any reflection in the 8 Å ≤ $d$ ≤ 140 Å angular domain, and we conclude that **L7**−**L10** exist as amorphous solids, which simply melt to give isotropic liquid phases. The associated complexes [Ln(**L*k***)$(NO_3)_3$] (**L*k*** = **L7**−**L10**; Ln = La, Pr, Eu, Lu) display similar behaviors with transitions around 110−120 °C (Figure S9 in the Supporting Information) prior to decomposition occurring at 170−175 °C (Table 3). The complexes [Ln(**L*k***)$(NO_3)_3$] (**L*k*** = **L11**−**L14**; Ln = La, Pr, Eu, Lu) are not mesomorphic and simply decompose when entering the isotropic liquid phase at 180−200 °C (Table 3). We thus focus our attention on the mesogenic properties of the complexes [Ln(**L*k***)$(NO_3)_3$] (Ln = La−Lu; **L*k*** = **L5** and **L6**) with the largest dendrimeric ligands.[10b,11] As found for the free ligands **L5** and **L6**, the associated complexes [Ln(**L*k***)$(NO_3)_3$] (Ln = La−Lu) enter a birefringent liquid-crystalline phase around 80−100 °C without displaying a pronounced peak in the DSC traces (Figure 10). SA-XRD profiles recorded for the complexes [Ln(**L5**)$(NO_3)_3$] (Ln = Eu, Gd, Tb, Lu) in the mesophase show two low-angle reflections with a 1:2 ratio, which are indexed as the (00$l$) reflections of a smectic phase with $d_{001} \cong 120$ Å and $d_{002} \cong 60$ Å (Figure S10 and Table S2 in the Supporting Information). The large interlayer distance given by the first harmonic of the smectic phase agrees with the approximate 119 Å length estimated by a simple molecular modeling of the monomeric complex [Ln(**L5**)$(NO_3)_3$] in its extended conformation (Figure S11 in the Supporting Information).[10b]

The molecular area (in Å$^2$) occupied by the rodlike cylinder at the interface between the layers in the smectic phases can be estimated with eq 10 ($V$ is the volume of the unit cell for $Z = 1$, MM is the molecular weight of the complex in g·mol$^{-1}$, $N_{av}$ is Avogadro's number in mol$^{-1}$, $\rho$ is the density in g·cm$^{-3}$ taken as $\rho = 1.0$ g·cm$^{-3}$ for the mesophase at 25 °C, and $\delta = V_{CH_2}(T)/V_{CH_2}(T^0)$ is a correcting factor for the dependence of $\rho$ with temperature, where $V_{CH_2}(T) = 0.02023T + 26.5616$ ($T$ is the experimental temperature in °C and $T^0 = 25$ °C).[29]

$$A = \frac{V}{d_{001}} = \frac{\mathrm{MM}\delta}{N_{\mathrm{Av}}\rho}\frac{1}{d_{001}} \times 10^{24} \qquad (10)$$

The experimental values measured for [Ln(**L5**)$(NO_3)_3$] (Ln = Eu, Gd, Tb, Lu) at $T = 100$ °C ($50 \le A \le 53$ Å$^2$; Table S2 in the Supporting Information) are only slightly larger than 44 Å$^2$ expected for the cross section of two closely packed parallel cyanobiphenyl segments.[30] We deduce that the rodlike complexes are arranged roughly perpendicularly to the interlayer interface, thus forming a bilayer smectic A2 mesophase in the 100−190 °C temperature range.[8a,31] The methylated complexes [Ln(**L6**)$(NO_3)_3$] (Ln = La, Pr, Eu, Gd, Tb, Y) also form smectic A2 phases around 90−110 °C (glass transition detected by POM and SA-XRD; Table 3 and Figure S12, in the

(29) Gehringer, L.; Bourgogne, C.; Guillon, D.; Donnio, B. *J. Am. Chem. Soc.* **2004**, *126*, 3856–3867.
(30) Guillon, D.; Skoulios, A. *Mol. Cryst. Liq. Cryst.* **1983**, *91*, 341–352.
(31) Guillon, D.; Skoulios, A. *J. Phys.* (*Paris*) **1984**, *45*, 607–621.

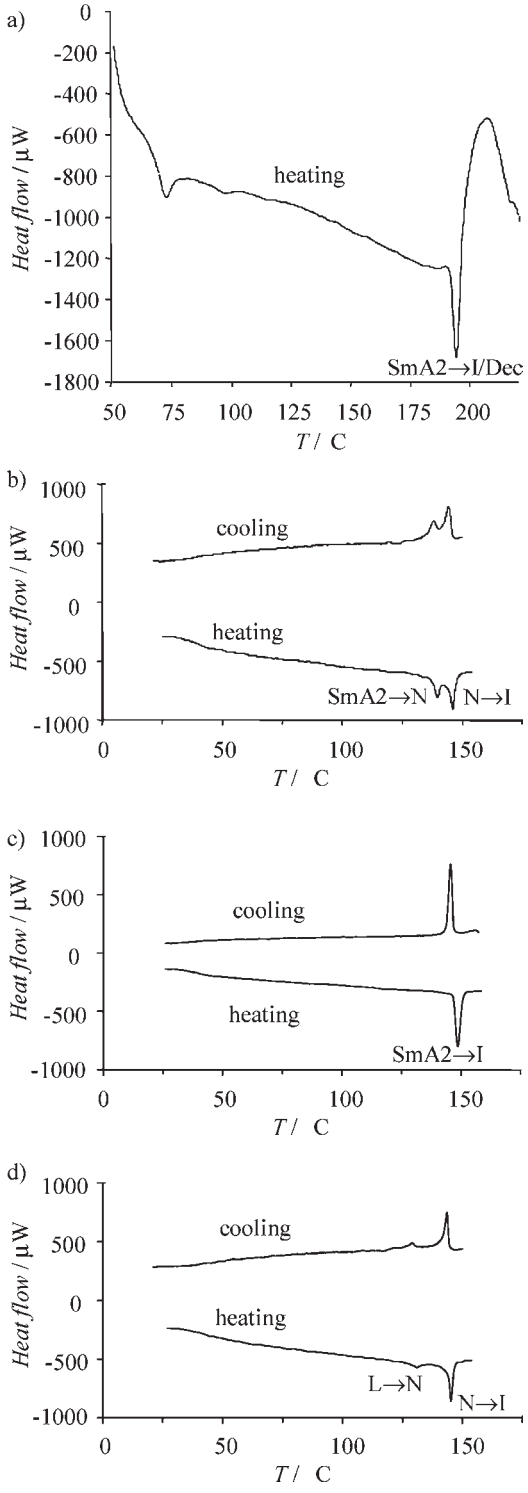


**Figure 10.** DSC traces recorded for the complexes (a) [Eu(**L5**)$(NO_3)_3$] (a single heating process), (b) [Eu(**L6**)$(NO_3)_3$], (c) [Pr(**L6**)$(NO_3)_3$], and (d) [Lu(**L6**)$(NO_3)_3$] (second heating/cooling cycle; SmA2 = bilayer smectic phase, N = nematic phase, L = lamellar phase, and I = isotropic liquid).

Supporting Information) with similar interlayer separations (100 Å $\leq d_{001} \leq$ 120 Å) but slightly larger molecular areas (60 Å$^2 \leq A \leq$ 66 Å$^2$) because of the expansion brought by the methyl groups in the packing of the terminal cyanobiphenyl groups (Table S3 in the Supporting Information). For the large lanthanides (Ln = La, Pr), the SmA2 phase is directly transformed into the isotropic

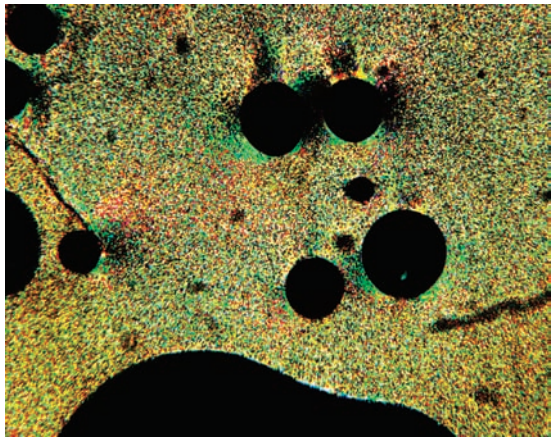

**Figure 11.** Birefringent texture observed by POM for [Eu(**L6**)$(NO_3)_3$] in the nematic mesophase.

liquid around 147−159 °C (Figure 10b), a clearing temperature approximately 30 °C lower than that found for the analogous nonmethylated complexes, which suggests less efficient intermolecular cohesion within the mesophase upon methylation of the terminal cyanobiphenyl groups. For the smaller lanthanides (Ln = Eu, Gd, Tb, Y), the initial SmA2 phase transforms into a second mesophase through a first-order phase transition prior to isotropization (Table 3 and Figures 10c and S13 in the Supporting Information). The breakdown of the $d_{001}$ and $d_{002}$ SA-XRD reflections combined with the appearance of Schlieren textures by POM (Figure 11) demonstrate the formation of a nematic phase for Ln = Eu, Y prior to isotropization.

Please note that the diffuse band attributed to some nonspecific residual intermolecular interactions between the aromatic segments responsible for the global alignment along the director $\vec{n}$ in the nematic phase is shifted by 1−5 Å on going from **L6** ($d \approx 17$ Å) to its complexes [Lu(**L6**)$(NO_3)_3$] ($d \approx 18-22$ Å; Table S3 in the Supporting Information), in line with a rigidification of the central aromatic core by metal complexation. For Ln = Gd and Tb, the DSC traces (Figure S13 in the Supporting Information) and the SA-XRD profiles (Figure S14 in the Supporting Information) imply first-order SmA2 → SmAd transitions,[8,28] in which the interlayer separation abruptly decreases by 10% because of partial interdigitation of the terminal cyanobiphenyl units (Table S3 in the Supporting Information). Interestingly, the complex with the smallest lanthanide [Lu(**L6**)$(NO_3)_3$] apparently shows the expected sequence g(90 °C)SmX(130 °C)N(144 °C)I (Figure 10d) but with an interlayer separation in the lamellar phase of only $d_{001} \cong 60$ Å (Table S3 and Figure S12 in the Supporting Information). This 50% reduction of the interlayer separation follows the trend initiated with Ln = Gd and Tb in the SmAd mesophase, and it is accompanied by the appearance of a diffuse reflection around $d \cong$ 9.0 Å (Figure S15 in the Supporting Information). From the molecular area $A = 116$ Å$^2$ estimated with eq 10 for [Lu(**L6**)$(NO_3)_3$] in this lamellar phase (L in Table S3 in the Supporting Information), we deduce that the ionic (i.e., metal-containing) and mesogenic (i.e., the cyanobiphenyl termini) parts of a pair of adjacent complexes separated by 9.0 Å contribute to the interface of interdigitated

molecules, forming the lamellar phase (Figure 9b). The total lack of a reflection at 9.0 Å for all other lanthanides (Ln = La−Tb; Figure S15 in the Supporting Information), or an extremely weak reflection for [Pr(**L6**)$(NO_3)_3$] (Table S3 in the Supporting Information), strongly suggests a larger separation between the packed rods within the layers of the SmA2 mesophase, in line with the packing of H-shaped dimers as schematically shown in Figure 9c. This observation is further supported by the detailed thermodynamic studies in a noncoordinating solvent, which show an increased propensity to form dimers for the larger lanthanides.

## Conclusion

Upon complexation of $Ln(NO_3)_3$ to the tridentate 5,5′-disubstituted 2,6[bis(*N*-ethylbenzimidazol-2-yl)pyridine] binding unit of the ligands **L5**−**L14** in noncoordinating dichloromethane, the monomeric complex [Ln(**L*k***)$(NO_3)_3$] is exclusively formed for the smallest lanthanide (Ln = Lu). For midrange (Ln = Eu) and for large lanthanides (Ln = Pr), the thermodynamic dimerization equilibria 2[Ln(**L*k***)$(NO_3)_3$] ↔ [$Ln_2$(**L*k***)$_2$-$(NO_3)_6$] can be investigated across the complete ligand series. Within the frame of a simple harmonic model, the formation of the dimer primarily results from the lanthanide-size-dependent building of intermetallic nitrato bridges, which are completed by nondirectional van der Waals interactions between the polarizable groups of the semidendrimeric ligand strands. Specific branching and methyl substitution of the ligand strands do influence the intermolecular interactions between the monomeric subunits, but enthalpy/entropy compensation strongly limits the effects of these structural changes on the global free energy of cohesion. In the absence of solvent, the situation completely changes and the ligands **L5**−**L14**, and the complexes [Ln(**L*k***)$(NO_3)_3$] with **L5**−**L6** display variable liquid-crystalline behaviors, which are dominated by the formation of smectic A and nematic phases. Detailed studies of the dendrimeric complexes [Ln(**L5**)$(NO_3)_3$] and [Ln(**L6**)$(NO_3)_3$] show that the large lanthanide cations (Ln = La, Pr) only produce bilayer smectic mesophases in the 90−180 °C range. Interestingly, the connection of methyl groups onto the terminal cyanobiphenyl groups in [Ln(**L6**)$(NO_3)_3$] is responsible for the appearance of either an additional interdigitated lamellar phase (Ln = Gd, Tb, Lu) or a nematic phase (Ln = Eu, Y, Lu) with midrange and small lanthanides. The intermolecular shift of the strands responsible for the decrease of the interlayer separation in the lamellar phases seems to be correlated with the propensity of the rodlike monomeric complexes to form dimer in solution. In other words, [Lu(**L6**)$(NO_3)_3$], which exists as a monomer in dichloromethane at millimolar concentration, leads to a lamellar mesophase in the pure compound with large interpenetration and short interlayer separations. On the other hand, [Ln(**L6**)$(NO_3)_3$] (Ln = Eu, Pr), which exists as a mixture of monomers and dimers in solution, leads to bilayer SmA2, with large interlayer distances matching the global shape of the extended complexes. We thus suspect that the disruption of the lateral intermolecular cohesion required for transforming a lamellar phase into a nematic phase in the pure complexes drastically depends on peripheral methyl substitution of the terminal cyanobiphenyl groups, while a similar effect is masked in solution by enthalpy/entropy compensation. Despite our reticence to develop tedious multistep synthetic strategies, it is clear that an unambiguous correlation between terminal methyl substitution (structural input) and the phase sequence in these dendrimeric complexes (thermodynamic output) would require the completion of family 1, initiated with **L5** and **L6**, with the systematic introduction of all accessible methyl-substituted cyanobiphenyl termini.

## Experimental Section

Chemicals were purchased from Fluka AG and Aldrich and used without further purification unless otherwise stated. The starting compounds 2,6-bis(1-ethyl-5-hydroxybenzimidazol-2-yl)pyridine,[14a] (4-cyano-2-methylphenyl)boronic acid,[13] 4-[(dimethylamino)pyridinium]-4-toluenesulfonate (DPTS),[32] 10-bromodecan-1-ol,[33] 4-(10-hydroxydecyloxy)benzoic acid,[10a] 5-(*tert*-butyldimethylsiloxy)isophthalic acid,[34] dimethyl-5-hydroxyisophthalate,[35] and ligands **L11**[10b] and **L5**[10b] were prepared by published procedures. The nitrate salts $Ln(NO_3)_3 \cdot xH_2O$ were prepared from the corresponding oxides (Aldrich, 99.99%).[36] The Ln content of the solid salt was determined by complexometric titrations with Titriplex III (Merck) in the presence of urotropine and xylene orange.[37] Acetonitrile and dichloromethane were distilled over calcium hydride. Silica-gel plates Merck 60 $F_{254}$ were used for thin-layer chromatography, and Fluka silica gel 60 (0.04−0.063 mm) was used for preparative column chromatography. Abbreviations: DCC = *N*,*N*′-dicyclohexylcarbodiimide, DPTS = 4-[(dimethylamino)pyridinium]-4-toluenesulfonate, 4-Ppy = 4-pyrrolidinopyridine, DMAP = 4-(dimethylamino)pyridine, EDCI = *N*-[3-(dimethylamino)propyl]-*N*′-ethylcarbodiimide, and dppf = 1,1′-bis(diphenylphosphino)ferrocene.

**Preparation of 4′-Hydroxy-3′-methyl-1,1′-biphenyl-4-carbonitrile (1).** A solution of 4-iodo-2-methylphenol (580 mg, 2.48 mmol), (4-cyanophenyl)boronic acid (0.40 g, 2.72 mmol, 1.1 equiv), and $K_3PO_4 \cdot H_2O$ (1.64 g, 7.12 mmol, 2.9 equiv) in 2-propanol (16 mL), and $H_2O$ (5 mL) was flushed with $N_2$ for 10 min. Pd(dppf)$Cl_2$ (40 mg, 0.049 mmol, 0.02 equiv) was added, and the solution was stirred under $N_2$ for 3 h at 70 °C. The solution was filtered, 40 mL of $CH_2Cl_2$ was added, and the phases were separated. The aqueous phase was extracted with 40 mL of $CH_2Cl_2$, and the combined organic phases were dried over $Na_2SO_4$, filtered, and evaporated to dryness. The crude product was purified by column chromatography (silica; $CH_2Cl_2/CH_3OH$ = 100/0 → 99.5/0.5) to yield 0.43 g (83%) of **1**.

$^1$H NMR ($CDCl_3$): $\delta$ 7.69 (d, 2H, $^3J$ = 8.5 Hz), 7.63 (d, 2H, $^3J$ = 8.6 Hz), 7.38 (d, 1H, $^4J$ = 2.7 Hz), 7.33 (dd, 1H, $^3J$ = 8.3 Hz, $^4J$ = 2.7 Hz), 6.87 (d, 1H, $^3J$ = 8.2 Hz), 4.86 (s, 1H), 2.33 (s, 3H). ESI-MS: *m*/*z* 210.3 ([M + H]$^+$), 227.5 ([M + $H_2O$ + H]$^+$), 436.5 ([2M + $H_2O$ + H]$^+$). Elem anal. Calcd for $C_{14}H_{11}NO \cdot 0.03H_2O$: C, 80.15; H, 5.31; N, 6.68. Found: C, 80.18; H, 5.33; N, 6.64.

**Preparation of 4′-Hydroxy-2′-methyl-1,1′-biphenyl-4-carbonitrile (2).** A solution of 4-bromo-3-methylphenol (1.16 g, 6.2 mmol), (4-cyanophenyl)boronic acid (1.00 g, 6.8 mmol, 1.1 equiv), and $K_3PO_4 \cdot H_2O$ (4.10 g, 17.8 mmol, 2.9 equiv) in 2-propanol (40 mL) and $H_2O$ (12 mL) was flushed with $N_2$ for 15 min. Pd(dppf)$Cl_2$ (100 mg, 0.12 mmol, 0.02 equiv) was added, and the solution was stirred under $N_2$ for 16 h at 70 °C. The solution was filtered, 2-propanol was evaporated, and 100 mL of half-saturated aqueous NaCl was added. The solution was extracted with 4 × 50 mL of $CH_2Cl_2$, and the combined organic phases were dried

(32) Noore, J. S.; Stupp, S. I. *Macromolecules* **1990**, *23*, 65–70.
(33) Chong, J. M.; Heuft, M. A.; Rabbat, P. *J. Org. Chem.* **2000**, *65*, 5837–5838.
(34) Miller, T. M.; Kwock, E. W.; Neenan, T. X. *Macromolecules* **1992**, *25*, 3143–3148.
(35) Li, F.-Y.; Zhu, L.-L.; Ma, X.; Wang, Q.-C.; Tian, H. *Tetrahedron Lett.* **2009**, *50*, 597–600.
(36) Desreux, J. F. In *Lanthanide Probes in Life, Chemical and Earth Sciences*; Bünzli, J.-C. G., Choppin, G. R., Eds.; Elsevier Publishing Co.: Amsterdam, The Netherlands, 1989; Chapter 2.
(37) Schwarzenbach, G. *Complexometirc Titrations*; Chapman and Hall: London, 1957; p 8.

over $Na_2SO_4$, filtered, and evaporated to dryness. The crude product was purified by column chromatography (silica; $CH_2Cl_2$/$CH_3OH$ = 100/0 → 99.5/0.5) to yield 0.87 g (67%) of **2**.

$^1$H NMR ($CDCl_3$): $\delta$ 7.69 (d, 2H, $^3J$ = 8.4 Hz), 7.40 (d, 2H, $^3J$ = 8.3 Hz), 7.08 (d, 1H, $^3J$ = 8.3 Hz), 6.78 (d, 1H, $^4J$ = 2.6 Hz), 6.75 (dd, 1H, $^3J$ = 8.3 Hz, $^4J$ = 2.6 Hz), 4.81 (s, 1H), 2.23 (s, 3H). ESI-MS: *m*/*z* 227.4 ([M + $H_2O$ + H]$^+$), 436.3 ([2M + $H_2O$ + H]$^+$). Elem anal. Calcd for $C_{14}H_{11}NO \cdot 0.11H_2O$: C, 79.59; H, 5.36; N, 6.63. Found: C, 79.61; H, 5.42; N, 6.46.

**Preparation of 4′-Hydroxy-2,2′-dimethyl-1,1′-biphenyl-4-carbonitrile (3).** A solution of 4-bromo-3-methylphenol (1.06 g, 5.65 mmol), (4-cyano-2-methylphenyl)boronic acid (1.00 g, 6.21 mmol, 1.1 equiv), and $K_3PO_4 \cdot H_2O$ (3.91 g, 17 mmol, 3.0 equiv) in 2-propanol (30 mL) and $H_2O$ (10 mL) was flushed with $N_2$ for 30 min. Pd(dppf)$Cl_2$ (90 mg, 0.113 mmol, 0.02 equiv) was added, and the solution was stirred under $N_2$ for 14 h at 70 °C. The solution was filtered, 2-propanol was evaporated, the aqueous phase was extracted with 4 × 50 mL of $CH_2Cl_2$, and the combined organic phases were dried over $Na_2SO_4$, filtered, and evaporated to dryness. The crude product was purified by column chromatography (silica; $CH_2Cl_2$/$CH_3OH$ = 100/0 → 99.5/0.5) to yield 0.75 g (59%) of **3**.

$^1$H NMR ($CDCl_3$): $\delta$ 7.56 (d, 1H, $^4J$ = 1.7 Hz), 7.50 (dd, 1H, $^3J$ = 8.2 Hz, $^4J$ = 1.7 Hz), 7.20 (d, 1H, $^3J$ = 7.9 Hz), 6.91 (d, 1H, $^3J$ = 8.0 Hz), 6.77 (d, 1H, $^4J$ = 2.8 Hz), 6.73 (dd, 1H, $^3J$ = 8.3 Hz, $^4J$ = 2.8 Hz), 4.86 (s, 1H), 2.09 (s, 3H), 1.98 (s, 3H). ESI-MS: *m*/*z* 222.3 ([M − H]$^-$). Elem anal. Calcd for $C_{15}H_{13}NO \cdot 0.05H_2O$: C, 80.37; H, 5.89; N, 6.25. Found: C, 80.37; H, 5.88; N, 6.22.

**Preparation of Compound 17.** To a solution of **1** (1.08 g, 5.16 mmol) in 100 mL of dry $CH_2Cl_2$ stirred at 0 °C was added 4-(10-hydroxydecyloxy)benzoic acid (1.52 g, 5.16 mmol), DCC (2.06 g, 10 mmol), DPTS (1.52 g, 5.16 mmol), and a spatula tip of 4-PPy. The reaction mixture was allowed to heat slowly to room temperature and stirred for 48 h. After filtration, the solution was evaporated to dryness and the residue was purified by column chromatography (silica; $CH_2Cl_2$/$CH_3OH$ = 100/0 → 99/1) to yield 2.28 g (91%) of **17**.

$^1$H NMR ($CDCl_3$): $\delta$ 8.18 (d, 2H, $^3J$ = 9.0 Hz), 7.73 (d, 2H, $^3J$ = 8.6 Hz), 7.68 (d, 2H, $^3J$ = 8.7 Hz), 7.49 (d, 1H, $^4J$ = 1.8 Hz), 7.46 (dd, 1H, $^3J$ = 8.3 Hz, $^4J$ = 2.2 Hz), 7.25 (d, 1H, $^3J$ = 8.5 Hz), 6.99 (d, 2H, $^3J$ = 9.0 Hz), 4.06 (t, 2H, $^3J$ = 6.5 Hz), 3.65 (t, 2H, $^3J$ = 6.5 Hz), 2.31 (s, 3H), 1.79−1.87 (m, 2H), 1.53−1.61 (m, 2H), 1.44−1.52 (m, 2H), 1.30−1.40 (m, 10H). ESI-MS: *m*/*z* 277.4 ([$HO(CH_2)_{10}OC_6H_4CO$]$^+$), 486.5 ([M + H]$^+$), 503.5 ([M + $H_2O$]$^+$), 508.6 ([M + Na]$^+$), 989.0 ([2M + $H_2O$]$^+$), 994.0 ([2M + Na]$^+$). Elem anal. Calcd for $C_{31}H_{35}NO_4 \cdot 0.18H_2O$: C, 76.16; H, 7.29; N, 2.87. Found: C, 76.07; H, 7.23; N, 2.83.

**Preparation of Compound 18.** To a solution of **2** (0.83 g, 3.97 mmol) in 100 mL of dry $CH_2Cl_2$ stirred at 0 °C was added 4-(10-hydroxydecyloxy)benzoic acid (1.17 g, 3.97 mmol), DCC (1.55 g, 7.5 mmol), DPTS (1.17 g, 3.97 mmol), and a spatula tip of 4-PPy. The reaction mixture was allowed to heat slowly to room temperature and stirred for 3 days. After filtration, the solution was evaporated to dryness and the residue was purified by column chromatography (silica; $CH_2Cl_2$/$CH_3OH$ = 100/0 → 99/1) to yield 1.59 g (82%) of **18**.

$^1$H NMR ($CDCl_3$): $\delta$ 8.15 (d, 2H, $^3J$ = 9.0 Hz), 7.72 (d, 2H, $^3J$ = 8.4 Hz), 7.45 (d, 2H, $^3J$ = 8.4 Hz), 7.24 (d, 1H, $^3J$ = 8.4 Hz), 7.15 (d, 1H, $^4J$ = 2.1 Hz), 7.11 (dd, 1H, $^3J$ = 8.5 Hz, $^4J$ = 2.4 Hz), 6.98 (d, 2H, $^3J$ = 8.8 Hz), 4.05 (t, 2H, $^3J$ = 6.5 Hz), 3.65 (q, 2H, $^3J$ = 6.1 Hz), 2.27 (s, 3H), 1.78−1.87 (m, 2H), 1.53−1.62 (m, 2H), 1.43−1.53 (m, 2H), 1.29−1.41 (m, 10H). ESI-MS: *m*/*z* 486.6 ([M + H]$^+$). Elem anal. Calcd for $C_{31}H_{35}NO_4$: C, 76.67; H, 7.26; N, 2.88. Found: C, 76.39; H, 7.29; N, 2.88.

**Preparation of Compound 19.** To a solution of 4-(10-hydroxydecyloxy)benzoic acid (0.70 g, 2.38 mmol) and **3** (0.53 g, 2.37 mmol) in 75 mL of freshly distilled $CH_2Cl_2$ cooled in an ice bath was added DCC (1.20 g, 5.83 mmol), DPTS (0.70 g, 2.38 mmol), and a spatula tip of 4-PPy. The reaction mixture was allowed to heat to room temperature and stirred for 16 h. After filtration and evaporation, the crude product was purified by column chromatography (silica; $CH_2Cl_2$/$CH_3OH$ = 100/0 → 99/1) to yield 1.06 g (90%) of **19**.

$^1$H NMR ($CDCl_3$): $\delta$ 8.15 (d, 2H, $^3J$ = 9.0 Hz), 7.58 (d, 1H, $^4J$ = 1.5 Hz), 7.54 (dd, 1H, $^3J$ = 8.0 Hz, $^4J$ = 1.5 Hz), 7.24 (d, 1H, $^3J$ = 7.9 Hz), 7.15 (m, 1H), 7.10 (m, 2H), 6.98 (d, 2H, $^3J$ = 9.0 Hz), 4.05 (t, 2H, $^3J$ = 6.6 Hz), 3.65 (t, 2H, $^3J$ = 6.3 Hz), 2.12 (s, 3H), 2.04 (s, 3H), 1.76−1.88 (m, 2H), 1.54−1.62 (m, 2H), 1.44−1.52 (m, 2H), 1.29−1.42 (m, 10 H). ESI-MS: *m*/*z* 500.5 ([M + H]$^+$), 277.6 ([$HO(CH_2)_{10}OC_6H_4CO$]$^+$). Elem anal. Calcd for $C_{32}H_{37}NO_4 \cdot 0.14H_2O$: C, 76.54; H, 7.48; N, 2.79. Found: C, 76.54; H, 7.54; N, 2.74.

**Preparation of Compound 21.** To a solution of **17** (1.46 g, 3.01 mmol) in 100 mL of dry $CH_2Cl_2$ stirred at 0 °C was added 4-carboxybenzaldehyde (0.45 g, 3.01 mmol), DCC (1.30 g, 6.31 mmol), DPTS (0.88 g, 3.01 mmol), and a spatula tip of 4-PPy. The reaction mixture was allowed to heat slowly to room temperature and stirred for 16 h. After filtration, the solution was evaporated to dryness and the residue was purified by column chromatography (silica; $CH_2Cl_2$/$CH_3OH$ = 100/0 → 99.5/0.5) to yield 1.46 g (78%) of **21**.

$^1$H NMR ($CDCl_3$): $\delta$ 10.10 (s, 1H), 8.20 (d, 2H, $^3J$ = 8.2 Hz), 8.17 (d, 2H, $^3J$ = 8.8 Hz), 7.96 (d, 2H, $^3J$ = 8.4 Hz), 7.73 (d, 2H, $^3J$ = 8.6 Hz), 7.68 (d, 2H, $^3J$ = 8.4 Hz), 7.49 (d, 1H, $^4J$ = 2.2 Hz), 7.46 (dd, 1H, $^3J$ = 8.6 Hz, $^4J$ = 2.2 Hz), 7.25 (d, 1H, $^3J$ = 8.6 Hz), 7.00 (d, 2H, $^3J$ = 9.0 Hz), 4.36 (t, 2H, $^3J$ = 6.7 Hz), 4.06 (t, 2H, $^3J$ = 6.7 Hz), 2.30 (s, 3H), 1.75−1.87 (m, 4H), 1.30−1.53 (m, 12H). ESI-MS: *m*/*z* 409.5 ([$CHOC_6H_4COO(CH_2)_{10}OC_6H_4CO$]$^+$, 618.3 ([M + H]$^+$), 635.2 ([M + $H_2O$]$^+$), 1253.3 ([2M + $H_2O$ + H]$^+$). Elem anal. Calcd for $C_{39}H_{39}NO_6$: C, 75.83; H, 6.36; N, 2.27. Found: C, 75.50; H, 6.40; N, 2.27.

**Preparation of Compound 22.** To a solution of **18** (1.49 g, 3.07 mmol) in 100 mL of dry $CH_2Cl_2$ stirred at 0 °C was added 4-carboxybenzaldehyde (0.46 g, 3.07 mmol), DCC (1.24 g, 6.00 mmol), DPTS (0.90 g, 3.07 mmol), and a spatula tip of 4-PPy. The reaction mixture was allowed to heat slowly to room temperature and stirred for 48 h. After filtration, the solution was evaporated to dryness and the residue was purified by column chromatography (silica; $CH_2Cl_2$/$CH_3OH$ = 100/0 → 99.5/0.5) to yield 1.22 g (64%) of **22**.

$^1$H NMR ($CDCl_3$): $\delta$ 10.10 (s, 1H), 8.20 (d, 2H, $^3J$ = 8.3 Hz), 8.15 (d, 2H, $^3J$ = 8.8 Hz), 7.95 (d, 2H, $^3J$ = 8.4 Hz), 7.72 (d, 2H, $^3J$ = 8.3 Hz), 7.45 (d, 2H, $^3J$ = 8.4 Hz), 7.24 (d, 1H, $^3J$ = 8.2 Hz), 7.15 (d, 1H, $^4J$ = 2.3 Hz), 7.11 (dd, 1H, $^3J$ = 8.5 Hz, $^4J$ = 2.4 Hz), 6.98 (d, 2H, $^3J$ = 9.0 Hz), 4.36 (t, 2H, $^3J$ = 6.7 Hz), 4.05 (t, 2H, $^3J$ = 6.6 Hz), 2.27 (s, 3H), 1.75−1.87 (m, 4H), 1.31−1.53 (m, 12H). ESI-MS: *m*/*z* 409.5 ([$CHOC_6H_4COO(CH_2)_{10}OC_6H_4CO$]$^+$, 618.5 ([M + H]$^+$), 635.7 ([M + $H_2O$]$^+$), 1253.3 ([2M + $H_2O$ + H]$^+$). Elem anal. Calcd for $C_{39}H_{39}NO_6 \cdot 0.19H_2O$: C, 75.41; H, 6.39; N, 2.25. Found: C, 75.41; H, 6.41; N, 2.18.

**Preparation of Compound 23.** A solution of 4-carboxybenzaldehyde (0.31 g, 2.06 mmol) and **19** (1.02 g, 2.04 mmol) in 200 mL of dry $CH_2Cl_2$ was cooled in an ice bath. DCC (0.90 g, 4.37 mmol), DPTS (0.60 g, 2.04 mmol), and a spatula tip of 4-PPy were added, and the reaction mixture was slowly heated to room temperature and stirred for 18 h. The solution was filtered, the solvent was evaporated, and the crude product was purified by column chromatography (silica; $CH_2Cl_2$/$CH_3OH$ = 100/0 → 99/1) to yield 1.16 g (90%) of **23**.

$^1$H NMR ($CDCl_3$): $\delta$ 10.10 (s, 1H), 8.20 (d, 2H, $^3J$ = 8.5 Hz), 8.15 (d, 2H, $^3J$ = 8.9 Hz), 7.95 (d, 2H, $^3J$ = 8.4 Hz), 7.58 (d, 1H, $^4J$ = 1.6 Hz), 7.55 (dd, 1H, $^3J$ = 8.2 Hz, $^4J$ = 1.6 Hz), 7.24 (d, 1H, $^3J$ = 8.1 Hz), 7.15 (m, 1H), 7.10 (m, 2H), 6.98 (d, 2H, $^3J$ = 8.9 Hz), 4.36 (t, 2H, $^3J$ = 6.7 Hz), 4.05 (t, 2H, $^3J$ = 6.6 Hz), 2.12 (s, 3H), 2.05 (s, 3H), 1.74−1.87 (m, 4H), 1.42−1.53 (m, 2H), 1.31−1.42 (m, 10 H). ESI-MS: *m*/*z* 632.5 ([M + H]$^+$), 409.4 ([$CHOC_6H_4COO(CH_2)_{10}OC_6H_4CO$]$^+$). Elem anal. Calcd for $C_{40}H_{41}NO_6 \cdot 0.97H_2O$: C, 74.01; H, 6.67; N, 2.16. Found: C, 74.00; H, 6.55; N, 2.16.

**Preparation of Compound 25.** To a solution of **21** (1.38 g, 2.23 mmol) in 75 mL of THF and 75 mL of $H_2O$ was added $NaClO_2$ (0.90 g, 10 mmol) and $H_2NSO_3H$ (0.97 g, 10 mmol). After stirring for 2 h, THF was evaporated and the aqueous phase was extracted with $CH_2Cl_2$ (3 × 50 mL). The combined organic extracts were dried over $Na_2SO_4$, filtered, and evaporated to dryness to yield 1.41 g (91%) of **25**.

$^1$H NMR (DMSO-$d_6$): $\delta$ 13.37 (s, 1H), 8.10 (d, 2H, $^3J$ = 8.5 Hz), 8.06 (s, 4H), 7.94 (d, 2H, $^3J$ = 9.1 Hz), 7.91 (d, 2H, $^3J$ = 9.0 Hz), 7.76 (d, 1H, $^4J$ = 2.2 Hz), 7.66 (dd, 1H, $^3J$ = 8.3 Hz, $^4J$ = 2.2 Hz), 7.33 (d, 1H, $^3J$ = 8.7 Hz), 7.12 (d, 2H, $^3J$ = 8.6 Hz), 4.30 (t, 2H, $^3J$ = 6.6 Hz), 4.09 (t, 2H, $^3J$ = 6.5 Hz), 2.23 (s, 3H), 1.68−1.79 (m, 4H), 1.26−1.46 (m, 12H). ESI-MS: $m/z$ 632.7 ([M − H]$^-$). Elem anal. Calcd for $C_{39}H_{39}NO_7 \cdot 0.46H_2O$: C, 72.97; H, 6.27; N, 2.18. Found: C, 72.97; H, 6.29; N, 2.12.

**Preparation of Compound 26.** To a solution of **22** (1.06 g, 1.72 mmol) in 75 mL of THF and 75 mL of $H_2O$ was added $NaClO_2$ (0.72 g, 8.0 mmol) and $H_2NSO_3H$ (0.78 g, 8.0 mmol). After stirring for 2 h, THF was evaporated and the aqueous phase was extracted with $CH_2Cl_2$ (4 × 50 mL). The combined organic extracts were dried over $Na_2SO_4$, filtered, and evaporated to dryness to yield 1.09 g (100%) of **26**.

$^1$H NMR (DMSO-$d_6$): $\delta$ 13.36 (s, 1H), 8.07 (d, 2H, $^3J$ = 9.0 Hz), 8.06 (s, 4H) 7.93 (d, 2H, $^3J$ = 8.4 Hz), 7.61 (d, 2H, $^3J$ = 8.2 Hz), 7.31 (d, 1H, $^3J$ = 8.3 Hz), 7.26 (d, 1H, $^4J$ = 2.2 Hz), 7.19 (dd, 1H, $^3J$ = 8.2 Hz, $^4J$ = 2.5 Hz), 7.11 (d, 2H, $^3J$ = 9.0 Hz), 4.30 (t, 2H, $^3J$ = 6.8 Hz), 4.08 (t, 2H, $^3J$ = 6.5 Hz), 2.26 (s, 3H), 1.68−1.78 (m, 4H), 1.27−1.46 (m, 12H). ESI-MS: $m/z$ 632.7 ([M − H]$^-$). Elem anal. Calcd for $C_{39}H_{39}NO_7 \cdot 0.45H_2O$: C, 72.98; H, 6.27; N, 2.18. Found: C, 72.99; H, 6.36; N, 2.02.

**Preparation of Compound 27.** To a solution of **23** (1.16 g, 1.84 mmol) in 50 mL of THF and 50 mL of $H_2O$ was added $NaClO_2$ (0.90 g, 10 mmol) and $H_2NSO_3H$ (0.97 g, 10 mmol). After stirring for 2 h, THF was evaporated and the aqueous phase was extracted with 3 × 50 mL of $CH_2Cl_2$. The combined organic extracts were dried over $Na_2SO_4$ and evaporated to yield 1.14 g (96%) of **27**.

$^1$H NMR (DMSO-$d_6$): $\delta$ 13.31 (s, 1H), 8.07 (d, 2H, $^3J$ = 8.8 Hz), 8.06 (s, 4H), 7.83 (d, 1H, $^4J$ = 1.5 Hz), 7.73 (dd, 1H, $^3J$ = 8.3 Hz, $^4J$ = 1.5 Hz), 7.33 (d, 1H, $^3J$ = 8.4 Hz), 7.25 (m, 1H), 7.16 (m, 2H), 7.11 (d, 2H, $^3J$ = 8.6 Hz), 4.30 (t, 2H, $^3J$ = 6.5 Hz), 4.08 (t, 2H, $^3J$ = 6.4 Hz), 2.07 (s, 3H), 2.01 (s, 3H), 1.68−1.78 (m, 4H), 1.26−1.45 (m, 12 H). ESI-MS: $m/z$ 646.9 ([M − H]$^-$). Elem anal. Calcd for $C_{40}H_{41}NO_7 \cdot 0.93H_2O$: C, 72.30; H, 6.50; N, 2.11. Found: C, 72.30; H, 6.50; N, 2.05.

**Preparation of Ligand L12.** To a solution of **25** (0.89 g, 1.40 mmol) in 100 mL of dry $CH_2Cl_2$ stirred at 0 °C was added 2,6-bis(1-ethyl-5-hydroxybenzimidazol-2-yl)pyridine (0.28 g, 0.70 mmol), DCC (0.62 g, 3.0 mmol), DPTS (0.41 g, 1.40 mmol), and a spatula tip of 4-PPy. The reaction mixture was allowed to heat slowly to room temperature and stirred for 48 h. After filtration, the solution was evaporated to dryness and the residue was purified by column chromatography (silica; $CH_2Cl_2$/$CH_3OH$ = 100/0 → 98.5/1.5) to yield 0.82 g (72%) of **L12**.

$^1$H NMR ($CDCl_3$): $\delta$ 8.36 (d, 2H, $^3J$ = 8.2 Hz), 8.34 (d, 4H, $^3J$ = 8.5 Hz), 8.20 (d, 4H, $^3J$ = 8.7 Hz), 8.17 (d, 4H, $^3J$ = 8.7 Hz), 8.08 (t, 1H, $^3J$ = 8.2 Hz), 7.72 (d, 4H, $^3J$ = 8.7 Hz), 7.71 (d, 2H, $^4J$ = 2.2 Hz), 7.67 (d, 4H, $^3J$ = 8.6 Hz), 7.52 (d, 2H, $^3J$ = 8.9 Hz), 7.49 (d, 2H, $^4J$ = 2.2 Hz), 7.46 (dd, 2H, $^3J$ = 8.2 Hz, $^4J$ = 2.4 Hz), 7.25 (d, 2H, $^3J$ = 8.8 Hz), 7.24 (d, 2H, $^3J$ = 8.7 Hz), 7.00 (d, 4H, $^3J$ = 8.9 Hz), 4.82 (q, 4H, $^3J$ = 7.3 Hz), 4.39 (t, 4H, $^3J$ = 6.8 Hz), 4.06 (t, 4H, $^3J$ = 6.5 Hz), 2.30 (s, 6H), 1.78−1.88 (m, 8H), 1.41 (t, 6H, $^3J$ = 7.3 Hz), 1.32−1.52 (m, 24H). ESI-MS: $m/z$ 1631.4 ([M + H]$^+$). Elem anal. Calcd for $C_{101}H_{95}N_7O_{14} \cdot H_2O$: C, 73.57; H, 5.93; N, 5.95. Found: C, 73.57; H, 6.03; N, 6.00.

**Preparation of Ligand L13.** To a solution of **26** (1.06 g, 1.67 mmol) in 100 mL of dry $CH_2Cl_2$ stirred at 0 °C was added 2,6-bis(1-ethyl-5-hydroxybenzimidazol-2-yl)pyridine (0.34 g, 0.84 mmol), DCC (0.82 g, 4.0 mmol), DPTS (0.49 g, 1.67 mmol), and a spatula tip of 4-PPy. The reaction mixture was allowed to heat slowly to room temperature and stirred for 48 h. After filtration, the solution was evaporated to dryness and the residue was purified by column chromatography (silica; $CH_2Cl_2$/$CH_3OH$ = 100/0 → 98.5/1.5) to yield 0.85 g (62%) of **L13**.

$^1$H NMR ($CDCl_3$): $\delta$ 8.36 (d, 2H, $^3J$ = 8.3 Hz), 8.34 (d, 4H, $^3J$ = 8.8 Hz), 8.20 (d, 4H, $^3J$ = 8.4 Hz), 8.15 (d, 4H, $^3J$ = 8.9 Hz), 8.08 (t, 1H, $^3J$ = 8.1 Hz), 7.72 (d, 4H, $^3J$ = 8.4 Hz), 7.71 (d, 2H, $^4J$ = 2.1 Hz), 7.52 (d, 2H, $^3J$ = 9.0 Hz), 7.45 (d, 4H, $^3J$ = 8.4 Hz), 7.25 (d, 2H, $^3J$ = 8.6 Hz), 7.24 (d, 2H, $^3J$ = 8.2 Hz), 7.14 (d, 2H, $^4J$ = 2.6 Hz), 7.11 (dd, 2H, $^3J$ = 8.5 Hz, $^4J$ = 2.6 Hz), 6.98 (d, 4H, $^3J$ = 8.7 Hz), 4.82 (q, 4H, $^3J$ = 7.2 Hz), 4.39 (t, 4H, $^3J$ = 6.7 Hz), 4.06 (t, 4H, $^3J$ = 6.5 Hz), 2.27 (s, 6H), 1.78−1.88 (m, 8H), 1.41 (t, 6H, $^3J$ = 7.3 Hz), 1.32−1.52 (m, 24H). ESI-MS: $m/z$ 1631.4 ([M + H]$^+$). Elem anal. Calcd for $C_{101}H_{95}N_7O_{14}$: C, 74.38; H, 5.87; N, 6.01. Found: C, 74.28; H, 5.93; N, 5.98.

**Preparation of Ligand L14.** To a solution of **27** (1.05 g, 1.62 mmol) and 2,6-bis(1-ethyl-5-hydroxybenzimidazol-2-yl)pyridine (0.32 g, 0.81 mmol) in 200 mL of dry $CH_2Cl_2$ stirred at 0 °C was added DCC (0.85 g, 4.13 mmol), DPTS (0.48 g, 1.63 mmol), and a spatula tip of 4-PPy. The reaction mixture was allowed to heat to room temperature and stirred for 18 h. After filtration, the solution was evaporated to dryness and the residue was purified by column chromatography (silica; $CH_2Cl_2$/$CH_3OH$ = 100/0 → 99/1) to yield 0.42 g (31%) of **L14**.

$^1$H NMR ($CDCl_3$): $\delta$ 8.37 (d, 2H, $^3J$ = 8.1 Hz), 8.34 (d, 4H, $^3J$ = 8.7 Hz), 8.20 (d, 4H, $^3J$ = 8.3 Hz), 8.15 (d, 4H, $^3J$ = 8.9 Hz), 8.09 (t, 1H, $^3J$ = 8.2 Hz), 7.72 (d, 2H, $^4J$ = 1.7 Hz), 7.58 (m, 2H), 7.53 (d, 2H, $^3J$ = 8.1 Hz), 7.53 (d, 2H, $^3J$ = 7.9 Hz), 7.26 (d, 2H, $^3J$ = 8.5 Hz), 7.23 (d, 2H, $^3J$ = 7.7 Hz), 7.15 (m, 2H), 7.10 (m, 4H), 6.99 (d, 4H, $^3J$ = 8.9 Hz), 4.82 (q, 4H, $^3J$ = 7.3 Hz), 4.38 (t, 4H, $^3J$ = 6.7 Hz), 4.06 (t, 4H, $^3J$ = 6.6 Hz), 2.12 (s, 6H), 2.04 (s, 6H), 1.70−1.87 (m, 8H), 1.44−1.53 (m, 8H), 1.41 (t, 6H, $^3J$ = 7.2 Hz), 1.32−1.41 (m, 16 H). ESI-MS: $m/z$ 1659.8 ([M + H]$^+$). Elem anal. Calcd for $C_{103}H_{99}N_7O_{14} \cdot 0.61H_2O$: C, 74.08; H, 6.05; N, 5.87. Found: C, 74.08; H, 6.24; N, 6.06.

**Preparation of Compound 28.** To a suspension of 60 g of $K_2CO_3$ in 250 mL of acetone was added 10-bromodecan-1-ol (13.35 g, 56.3 mmol), dimethyl 5-hydroxyisophthalate (11.83 g, 56.3 mmol), and a spatula tip of KI. The reaction mixture was refluxed for 68 h, the acetone was evaporated, and the aqueous phase was extracted with 3 × 100 mL of ethyl acetate. The combined organic extracts were dried over $Na_2SO_4$, filtered, and evaporated to dryness. The crude ester was purified by column chromatography (silica; $CH_2Cl_2$/$CH_3OH$ = 100/0 → 99/1) and dissolved in 225 mL of EtOH. To this was added 150 mL of 1 M KOH, and the solution was stirred for 2 h. After evaporation of ethanol, the aqueous solution was washed with 2 × 100 mL of $CH_2Cl_2$ and acidified to pH = 1 with 2 M HCl. The resulting white precipitate was filtered off, washed with aqueous 0.1 M HCl, and dried in vacuum to yield 6.15 g (32%) of **28**.

$^1$H NMR (DMSO-$d_6$): $\delta$ 13.28 (s, 2H), 8.06 (t, 1H, $^4J$ = 1.4 Hz), 7.62 (d, 2H, $^4J$ = 1.4 Hz), 4.06 (t, 2H, $^3J$ = 6.6 Hz), 3.36 (t, 2H, $^3J$ = 6.7 Hz), 1.67−1.77 (m, 2H), 1.36−1.46 (m, 4H), 1.22−1.36 (m, 10H). ESI- MS: $m/z$ 337.3 ([M − H]$^-$). Elem anal. Calcd for $C_{18}H_{26}O_6 \cdot 0.58H_2O$: C, 61.97; H, 7.85. Found: C, 61.95; H, 7.51.

**Preparation of Compound 4.** To a mixture of **28** (1.35 g, 3.99 mmol) and 4′-hydroxybiphenyl-4-carbonitrile (1.56 g, 7.99 mmol) in 200 mL of dry $CH_2Cl_2$ cooled in an ice bath was added DCC (3.80 g, 18.45 mmol), DPTS (2.35 g, 7.99 mmol), and a spatula tip of 4-PPy. The reaction mixture was allowed to warm to room temperature and stirred for 18 h. After filtration and evaporation of the solvent, the crude product was purified by column chromatography (silica; $CH_2Cl_2$/$CH_3OH$ = 100/0 → 99/1) to yield 2.24 g (81%) of **4**.

$^1$H NMR ($CDCl_3$): $\delta$ 8.62 (t, 1H, $^4J$ = 1.5 Hz), 7.99 (d, 2H, $^4J$ = 1.4 Hz), 7.75 (d, 4H, $^3J$ = 8.3 Hz), 7.70 (d, 4H, $^3J$ = 8.4 Hz), 7.67 (d, 4H, $^3J$ = 8.6 Hz), 7.38 (d, 4H, $^3J$ = 8.6 Hz), 4.13 (t, 2H,

$^3J$ = 6.4 Hz), 3.64 (t, 2H, $^3J$ = 6.6 Hz), 1.82−1.90 (m, 2H), 1.46−1.61 (m, 4H), 1.30−1.43 (m, 10H). ESI-MS: *m*/*z* 693.5 ([M + H]$^+$). Elem anal. Calcd for $C_{44}H_{40}N_2O_6 \cdot 1.09H_2O$: C, 74.18; H, 5.97; N, 3.93. Found: C, 74.18; H, 6.02; N, 3.91.

**Preparation of Compound 5.** To a solution of **28** (1.26 g, 3.72 mmol) and **1** (1.56 g, 7.46 mmol) in 50 mL of dry $CH_2Cl_2$ cooled in an ice bath was added DCC (4.12 g, 20 mmol), DPTS (2.19 g, 7.45 mmol), and a spatula tip of 4-PPy. After 2 h, the ice bath was removed and the reaction mixture was stirred for 2 days, filtered, and evaporated to dryness. The crude product was purified by column chromatography (silica; $CH_2Cl_2/CH_3OH$ = 100/0 → 99.5/0.5) to yield 1.22 g (46%) of **5**.

$^1$H NMR ($CDCl_3$): $\delta$ 8.66 (t, 1H, $^4J$ = 1.5 Hz), 8.01 (d, 2H, $^4J$ = 1.5 Hz), 7.74 (d, 4H, $^3J$ = 8.3 Hz), 7.69 (d, 4H, $^3J$ = 8.4 Hz), 7.52 (d, 2H, $^4J$ = 1.9 Hz), 7.49 (dd, 2H, $^3J$ = 8.3 Hz, $^4J$ = 2.0 Hz), 7.28 (d, 2H, $^3J$ = 8.3 Hz), 4.14 (t, 2H, $^3J$ = 6.4 Hz), 3.64 (t, 2H, $^3J$ = 6.6 Hz), 2.34 (s, 6H), 1.80−1.92 (m, 4H), 1.30−1.60 (m, 12H). ESI-MS: *m*/*z* 721.8 ([M + H]$^+$). Elem anal. Calcd for $C_{46}H_{44}N_2O_6 \cdot 0.40H_2O$: C, 75.89; H, 6.20; N, 3.85. Found: C, 75.91; H, 6.28; N, 3.60.

**Preparation of Compound 6.** A solution of **28** (0.29 g, 0.86 mmol) and **2** (0.36 g, 1.72 mmol) in 50 mL of freshly distilled $CH_2Cl_2$ was cooled in an ice bath. DCC (0.82 g, 3.98 mmol), DPTS (0.51 g, 1.73 mmol), and a spatula tip of 4-PPy were added, and the ice bath was removed. After stirring for 24 h at room temperature, the solution was filtered and evaporated to dryness. Purification by column chromatography (silica; $CH_2Cl_2/CH_3OH$ = 100/0 → 99.4/0.6) gave 0.52 g (84%) of **6**.

$^1$H NMR ($CDCl_3$): $\delta$ 8.61 (t, 1H, $^4J$ = 1.5 Hz), 7.98 (d, 2H, $^4J$ = 1.5 Hz), 7.73 (d, 4H, $^3J$ = 8.1 Hz), 7.46 (d, 4H, $^3J$ = 8.2 Hz), 7.27 (d, 2H, $^3J$ = 8.5 Hz), 7.19 (d, 2H, $^4J$ = 2.3 Hz), 7.16 (dd, 2H, $^3J$ = 8.3 Hz, $^4J$ = 2.4 Hz), 4.13 (t, 2H, $^3J$ = 6.5 Hz), 3.64 (t, 2H, $^3J$ = 6.7 Hz), 2.29 (s, 6H), 1.75−1.90 (m, 4H), 1.44−1.61 (m, 4H), 1.27−1.43 (m, 8H). ESI-MS: *m*/*z* 721.7 ([M + H]$^+$). Elem anal. Calcd for $C_{46}H_{44}N_2O_6 \cdot 1.05H_2O$: C, 74.68; H, 6.28; N, 3.79. Found: C, 74.70; H, 6.28; N, 3.39.

**Preparation of Compound 7.** A suspension of **3** (0.66 g, 2.96 mmol) and **28** (0.50 g, 1.48 mmol) in 50 mL of freshly distilled $CH_2Cl_2$ was cooled in an ice bath. After the addition of DCC (1.50 g, 7.28 mmol), DPTS (0.87 g, 2.96 mmol), and a spatula tip of 4-PPy, the reaction mixture was allowed to warm slowly and was stirred for 16 h at room temperature. The filtered solution was evaporated to dryness and purified by column chromatography (silica; $CH_2Cl_2/CH_3OH$ = 100/0 → 99/1) to yield 1.00 g (90%) of **7**.

$^1$H NMR ($CDCl_3$): $\delta$ 8.62 (t, 1H, $^4J$ = 1.5 Hz), 7.98 (d, 2H, $^4J$ = 1.5 Hz), 7.59 (s, 2H), 7.55 (d, 2H, $^3J$ = 7.9 Hz), 7.25 (d, 2H, $^3J$ = 8.1 Hz), 7.19 (m, 2H), 7.11−7.17 (m, 4H), 4.12 (t, 2H, $^3J$ = 6.5 Hz), 3.64 (t, 2H, $^3J$ = 6.7 Hz), 2.13 (s, 6H), 2.07 (s, 6H), 1.81−1.92 (m, 2H), 1.46−1.55 (m, 4H), 1.30−1.42 (m, 10H). ESI-MS: *m*/*z* 749.5 ([M + H]$^+$).Elem anal. Calcd for $C_{48}H_{48}N_2O_6 \cdot 2.07H_2O$: C, 73.32; H, 6.69; N, 3.56. Found: C, 73.31; H, 6.39; N, 3.43.

**Preparation of Compound 8.** 4-Carboxybenzaldehyde (0.49 g, 3.26 mmol) and **4** (2.28 g, 3.29 mmol) in 200 mL of dry $CH_2Cl_2$ were stirred in an ice bath. DCC (1.65 g, 8.01 mmol), DPTS (0.96 g, 3.27 mmol), and a spatula tip of 4-PPy were added. The reaction mixture was allowed to warm slowly to room temperature, stirred for 19 h, and filtered. Purification by column chromatography (silica; $CH_2Cl_2/CH_3OH$ = 100/0 → 99.5/0.5) gave 2.17 g (81%) of **8**.

$^1$H NMR ($CDCl_3$): $\delta$ 10.10 (s, 1H), 8.63 (t, 1H, $^4J$ = 1.5 Hz), 8.20 (d, 2H, $^3J$ = 8.5 Hz), 7.99 (d, 2H, $^4J$ = 1.5 Hz), 7.95 (d, 2H, $^3J$ = 8.4 Hz), 7.75 (d, 4H, $^3J$ = 8.4 Hz), 7.70 (d, 4H, $^3J$ = 8.5 Hz), 7.67 (d, 4H, $^3J$ = 8.8 Hz), 7.37 (d, 4H, $^3J$ = 8.6 Hz), 4.35 (t, 2H, $^3J$ = 6.8 Hz), 4.13 (t, 2H, $^3J$ = 6.6 Hz), 1.75−1.90 (m, 4H), 1.32−1.90 (m, 12H). ESI-MS: *m*/*z* 825.7 ([M + H]$^+$). Elem anal. Calcd for $C_{52}H_{44}N_2O_8$: C, 75.71; H, 5.38; N, 3.40. Found: C, 75.53; H, 5.42; N, 3.34.

**Preparation of Compound 9.** To a solution of 4-carboxybenzaldehyde (0.26 g, 1.73 mmol) and **5** (1.22 g, 1.69 mmol) in 50 mL of freshly distilled $CH_2Cl_2$ stirred in an ice bath was added DCC (1.02 g, 4.95 mmol), DPTS (0.50 g, 1.70 mmol), and a spatula tip of 4-PPy. The reaction mixture was allowed to warm slowly to room temperature, stirred for 16 h, and filtered. Purification by column chromatography (silica; $CH_2Cl_2/CH_3OH$ = 100/0 → 99.5/0.5) gave 1.01 g (70%) of **9**.

$^1$H NMR ($CDCl_3$): $\delta$ 10.09 (s, 1H), 8.66 (t, 1H, $^4J$ = 1.5 Hz), 8.19 (d, 2H, $^3J$ = 8.4 Hz), 8.01 (d, 2H, $^4J$ = 1.5 Hz), 7.95 (d, 2H, $^3J$ = 8.5 Hz), 7.74 (d, 4H, $^3J$ = 8.6 Hz), 7.69 (d, 4H, $^3J$ = 8.6 Hz), 7.52 (d, 2H, $^4J$ = 2.2 Hz), 7.49 (dd, 2H, $^3J$ = 8.3 Hz, $^4J$ = 2.0 Hz), 7.28 (d, 2H, $^3J$ = 8.3 Hz), 4.35 (t, 2H, $^3J$ = 6.7 Hz), 4.13 (t, 2H, $^3J$ = 6.4 Hz), 2.34 (s, 6H), 1.74−1.92 (m, 4H), 1.28−1.55 (m, 12H). ESI-MS: *m*/*z* 853.5 ([M + H]$^+$). Elem anal. Calcd for $C_{54}H_{48}N_2O_8 \cdot 1.30H_2O$: C, 74.01; H, 5.82; N, 3.20. Found: C, 74.01; H, 5.80; N, 3.05.

**Preparation of Compound 10.** A solution of 4-carboxybenzaldehyde (0.11 g, 0.73 mmol) and **6** (0.52 g, 0.72 mmol) in 50 mL of freshly distilled $CH_2Cl_2$ was stirred in an ice bath. DCC (0.40 g, 1.94 mmol), DPTS (0.21 g, 0.71 mmol), and a spatula tip of 4-PPy were added. The ice bath was allowed to melt, and the reaction mixture was stirred for 16 h at room temperature before being filtered. Purification by column chromatography (silica; $CH_2Cl_2/CH_3OH$ = 100/0 → 99.5/0.5) gave 0.32 g (52%) of **10**.

$^1$H NMR ($CDCl_3$): $\delta$ 10.09 (s, 1H), 8.61 (t, 1H, $^4J$ = 1.5 Hz), 8.19 (d, 2H, $^3J$ = 8.2 Hz), 7.98 (d, 2H, $^4J$ = 1.5 Hz), 7.95 (d, 2H, $^3J$ = 8.3 Hz), 7.73 (d, 4H, $^3J$ = 8.1 Hz), 7.46 (d, 4H, $^3J$ = 8.2 Hz), 7.27 (d, 2H, $^3J$ = 8.3 Hz), 7.19 (d, 2H, $^4J$ = 2.1 Hz), 7.15 (dd, 2H, $^3J$ = 8.2 Hz, $^4J$ = 2.1 Hz), 4.36 (t, 2H, $^3J$ = 6.9 Hz), 4.12 (t, 2H, $^3J$ = 6.5 Hz), 2.29 (s, 6H), 1.74−1.90 (m, 4H), 1.42−1.55 (m, 4H), 1.28−1.42 (m, 8H). ESI-MS: *m*/*z* 853.4 ([M + H]$^+$). Elem anal. Calcd for $C_{54}H_{48}N_2O_8 \cdot 1.58H_2O$: C, 73.59; H, 5.85; N, 3.18. Found: C, 73.61; H, 6.06; N, 2.94.

**Preparation of Compound 11.** A solution of 4-carboxybenzaldehyde (0.17 g, 1.13 mmol) and **7** (0.84 g, 1.12 mmol) in 75 mL of dry $CH_2Cl_2$ was cooled in an ice bath. To this solution were added DCC (0.62 g, 3.01 mmol), DPTS (0.33 g, 1.12 mmol), and a spatula tip of 4-PPy. After being allowed to slowly heat to room temperature, the reaction mixture was stirred for 19 h and filtered. Purification by column chromatography (silica; $CH_2Cl_2/CH_3OH$ = 100/0 → 99.5/0.5) gave 0.83 g (84%) of **11**.

$^1$H NMR ($CDCl_3$): $\delta$ 10.10 (s, 1H), 8.62 (t, 1H, $^4J$ = 1.5 Hz), 8.20 (d, 2H, $^3J$ = 8.3 Hz), 7.98 (d, 2H, $^4J$ = 1.5 Hz), 7.95 (d, 2H, $^3J$ = 8.5 Hz), 7.59 (d, 2H, $^4J$ = 1.7 Hz), 7.55 (dd, 2H, $^3J$ = 7.9 Hz, $^4J$ = 1.7 Hz), 7.25 (d, 2H, $^3J$ = 7.9 Hz), 7.19 (m, 2H), 7.11−7.17 (m, 4H), 4.36 (t, 2H, $^3J$ = 6.7 Hz), 4.12 (t, 2H, $^3J$ = 6.7 Hz), 2.13 (s, 6H), 2.07 (s, 6H), 1.75−1.92 (m, 4H), 1.32−1.55 (m, 12H). ESI-MS: *m*/*z* 898.3 ([M + $NH_4$]$^+$). Elem anal. Calcd for $C_{56}H_{52}N_2O_8 \cdot 1.10H_2O$: C, 74.67; H, 6.06; N, 3.11. Found: C, 74.66; H, 5.91; N, 3.05.

**Preparation of Compound 12.** To a solution of **8** (2.17 g, 2.63 mmol) in 50 mL of THF and 50 mL of $H_2O$ was added $NaClO_2$ (1.36 g, 15.0 mmol) and $H_2NSO_3H$ (1.46 g, 15.0 mmol). After stirring for 3 h, THF was evaporated and the aqueous phase was extracted with 4 × 50 mL of $CH_2Cl_2$. The combined extracts were dried over $Na_2SO_4$, filtered, and evaporated to dryness to yield 2.16 g (98%) of **12**.

$^1$H NMR ($CDCl_3$): $\delta$ 8.62 (t, 1H, $^4J$ = 1.5 Hz), 8.16 (d, 2H, $^3J$ = 8.2 Hz), 8.12 (d, 2H, $^3J$ = 8.3 Hz), 7.99 (d, 2H, $^4J$ = 1.5 Hz), 7.75 (d, 4H, $^3J$ = 8.4 Hz), 7.70 (d, 4H, $^3J$ = 8.4 Hz), 7.67 (d, 4H, $^3J$ = 8.7 Hz), 7.37 (d, 4H, $^3J$ = 8.8 Hz), 4.35 (t, 2H, $^3J$ = 6.6 Hz), 4.13 (t, 2H, $^3J$ = 6.5 Hz), 1.75−1.90 (m, 4H), 1.30−1.55 (m, 12H). ESI-MS: *m*/*z* 839.7 ([M − H]$^-$). Elem anal. Calcd for $C_{52}H_{44}N_2O_9 \cdot 1.27H_2O$: C, 72.31; H, 5.43; N, 3.24. Found: C, 72.32; H, 5.46; N, 3.09.

**Preparation of Compound 13.** A solution of **9** (1.01 g, 1.18 mmol), $NaClO_2$ (0.90 g, 10.0 mmol), and $H_2NSO_3H$ (0.97 g, 10.0 mmol) in 50 mL of THF and 50 mL of $H_2O$ was stirred for 3 h.

THF was evaporated, and the aqueous phase was extracted with 3 × 50 mL of $CH_2Cl_2$. The combined extracts were dried over $Na_2SO_4$, filtered, and evaporated to dryness to yield 1.00 g (98%) of **13**.

$^1$H NMR ($CDCl_3$): $\delta$ 8.65 (t, 1H, $^4J$ = 1.4 Hz), 8.15 (d, 2H, $^3J$ = 8.4 Hz), 8.11 (d, 2H, $^3J$ = 8.4 Hz), 8.01 (d, 2H, $^4J$ = 1.4 Hz), 7.73 (d, 4H, $^3J$ = 8.3 Hz), 7.68 (d, 4H, $^3J$ = 8.4 Hz), 7.51 (d, 2H, $^4J$ = 2.2 Hz), 7.49 (dd, 2H, $^3J$ = 8.3 Hz, $^4J$ = 2.2 Hz), 7.27 (d, 2H, $^3J$ = 8.2 Hz), 4.35 (t, 2H, $^3J$ = 6.7 Hz), 4.13 (t, 2H, $^3J$ = 6.3 Hz), 2.33 (s, 6H), 1.74−1.90 (m, 4H), 1.30−1.56 (m, 12H). ESI-MS: *m*/*z* 867.7 ([M − H]$^-$). Elem anal. Calcd for $C_{54}H_{48}N_2O_9 \cdot 1.97H_2O$: C, 71.72; H, 5.79; N, 3.10. Found: C, 71.73; H, 5.91; N, 2.97.

**Preparation of Compound 14.** To a solution of **10** (0.32 g, 0.37 mmol) in 25 mL of THF and 25 mL of $H_2O$ was added $NaClO_2$ (0.18 g, 2.0 mmol) and $H_2NSO_3H$ (0.19 g, 2.0 mmol). After stirring for 2 h at room temperature, THF was evaporated and the aqueous solution extracted with $CH_2Cl_2$ (3 × 25 mL). Evaporation yielded 0.30 g (92%) of **14**.

$^1$H NMR ($CDCl_3$): $\delta$ 8.61 (t, 1H, $^4J$ = 1.5 Hz), 8.11−8.17 (m, 4H), 7.98 (d, 2H, $^4J$ = 1.5 Hz), 7.73 (d, 4H, $^3J$ = 8.2 Hz), 7.46 (d, 4H, $^3J$ = 8.3 Hz), 7.27 (d, 2H, $^3J$ = 8.4 Hz), 7.19 (d, 2H, $^4J$ = 2.2 Hz), 7.15 (dd, 2H, $^3J$ = 8.4 Hz, $^4J$ = 2.3 Hz), 4.35 (t, 2H, $^3J$ = 6.7 Hz), 4.12 (t, 2H, $^3J$ = 6.7 Hz), 2.29 (s, 6H), 1.75−1.89 (m, 4H), 1.42−1.54 (m, 4H), 1.30−1.42 (m, 8H). ESI-MS: *m*/*z* 867.7 ([M − H]$^-$). Elem anal. Calcd for $C_{54}H_{48}N_2O_9 \cdot 2.58H_2O$: C, 70.84; H, 5.85; N, 3.06. Found: C, 70.86; H, 6.02; N, 2.95.

**Preparation of Compound 15.** A solution of **11** (0.83 g, 0.94 mmol), $NaClO_2$ (0.45 g, 5.0 mmol), and $H_2NSO_3H$ (0.49 g, 5.0 mmol) in 50 mL of THF and 50 mL of $H_2O$ was stirred for 4 h. THF was evaporated, and the aqueous phase was extracted with 3 × 150 mL of $CH_2Cl_2$. The combined organic extracts were dried over $Na_2SO_4$, filtered, and evaporated to dryness. Yield: 0.79 g (93%) of **15**.

$^1$H NMR ($CDCl_3$): $\delta$ 8.61 (t, 1H, $^4J$ = 1.5 Hz), 8.16 (d, 2H, $^3J$ = 8.3 Hz), 8.13 (d, 2H, $^3J$ = 8.4 Hz), 7.98 (d, 2H, $^4J$ = 1.4 Hz), 7.59 (d, 2H, $^4J$ = 1.5 Hz), 7.55 (dd, 2H, $^3J$ = 7.7 Hz, $^4J$ = 1.4 Hz), 7.25 (d, 2H, $^3J$ = 7.8 Hz), 7.19 (m, 2H), 7.11−7.17 (m, 4H), 4.35 (t, 2H, $^3J$ = 6.9 Hz), 4.12 (t, 2H, $^3J$ = 6.5 Hz), 2.13 (s, 6H), 2.07 (s, 6H), 1.77−1.84 (m, 4H), 1.29−1.53 (m, 12H). ESI-MS: *m*/*z* 895.1 ([M − H]$^-$). Elem anal. Calcd for $C_{56}H_{52}N_2O_9 \cdot 1.07H_2O$: C, 73.40; H, 5.96; N, 3.06. Found: C, 73.43; H, 6.27; N, 2.84.

**Preparation of Ligand L7.** A solution of 2,6-bis(1-ethyl-5-hydroxybenzimidazol-2-yl)pyridine (0.20 g, 0.50 mmol), **12** (0.84 g, 1.0 mmol), EDCI·HCl (0.60 g, 3.13 mmol), and DMAP (0.38 g, 3.11 mmol) in 50 mL of freshly distilled $CH_2Cl_2$ was refluxed under $N_2$ for 16 h. After washing with 3 × 50 mL of a saturated aqueous NaCl solution, the organic phase was dried over $Na_2SO_4$, filtered, and evaporated. Purification by column chromatography (silica; $CH_2Cl_2/CH_3OH$ = 100/0 → 98.5/1.5) gave 0.45 g (44%) of **L7**.

$^1$H NMR ($CDCl_3$): $\delta$ 8.62 (t, 2H, $^4J$ = 1.4 Hz), 8.42 (d, 2H, $^3J$ = 8.5 Hz), 8.32 (d, 4H, $^3J$ = 8.5 Hz), 8.19 (d, 4H, $^3J$ = 8.5 Hz), 8.12 (d, 2H, $^3J$ = 8.5 Hz), 7.99 (d, 4H, $^4J$ = 1.5 Hz), 7.75 (d, 8H, $^3J$ = 8.3 Hz), 7.75 (d, 2H, $^3J$ = 8.3 Hz), 7.69 (d, 8H, $^3J$ = 8.5 Hz), 7.67 (d, 8H, $^3J$ = 8.8 Hz), 7.54 (d, 2H, $^3J$ = 8.8 Hz), 7.37 (d, 8H, $^3J$ = 8.7 Hz), 7.27 (d, 2H, $^3J$ = 8.8 Hz), 4.38 (t, 4H, $^3J$ = 6.6 Hz), 4.14 (t, 4H, $^3J$ = 6.5 Hz), 1.77−1.92 (m, 8H), 1.32−1.55 (m, 24H). ESI-MS: *m*/*z* 2044.9 ([M + H]$^+$). Elem anal. Calcd for $C_{127}H_{105}N_9O_{18} \cdot 2.72H_2O$: C, 72.84; H, 5.32; N, 6.02. Found: C, 72.84; H, 5.18; N, 5.83.

**Preparation of Ligand L8.** A solution of **13** (0.52 g, 0.60 mmol), 2,6-bis(1-ethyl-5-hydroxybenzimidazol-2-yl)pyridine (0.12 g, 0.30 mmol), EDCI·HCl (0.38 g, 2.0 mmol), and DMAP (0.24 g, 2 mmol) in 50 mL of dry $CH_2Cl_2$ was refluxed under $N_2$ for 18 h. The solution was washed with 3 × 50 mL of a saturated aqueous NaCl solution, and the organic phase was dried over $Na_2SO_4$, filtered, and evaporated. The crude product was purified by column chromatography (silica; $CH_2Cl_2/CH_3OH$ = 100/0 → 98.5/1.5) to yield 0.19 g (30%) of **L8**.

$^1$H NMR ($CDCl_3$): $\delta$ 8.66 (t, 2H, $^4J$ = 1.4 Hz), 8.61 (d, 2H, $^3J$ = 8.4 Hz), 8.32 (d, 4H, $^3J$ = 8.5 Hz), 8.26 (t, 1H, $^3J$ = 8.4 Hz), 8.20 (d, 4H, $^3J$ = 8.4 Hz), 8.02 (d, 4H, $^4J$ = 1.5 Hz), 7.89 (d, 2H, $^4J$ = 1.8 Hz), 7.74 (d, 8H, $^3J$ = 8.5 Hz), 7.69 (d, 8H, $^3J$ = 8.5 Hz), 7.62 (d, 2H, $^3J$ = 9.1 Hz), 7.52 (d, 4H, $^4J$ = 2.0 Hz), 7.49 (dd, 4H, $^3J$ = 8.3 Hz, $^4J$ = 2.0 Hz), 7.38 (dd, 2H, $^3J$ = 9.0 Hz, $^4J$ = 1.9 Hz), 7.29 (d, 4H, $^3J$ = 8.4 Hz), 4.85 (q, 4H, $^3J$ = 7.0 Hz), 4.38 (t, 4H, $^3J$ = 6.7 Hz), 4.15 (t, 4H, $^3J$ = 6.4 Hz), 2.34 (s, 12H), 1.77−1.92 (m, 8H), 1.48 (t, 6H, $^3J$ = 7.2 Hz), 1.30−1.58 (m, 24H). ESI-MS: *m*/*z* 2101.2 ([M + H]$^+$). Elem anal. Calcd for $C_{131}H_{113}N_9O_{18} \cdot 1.07H_2O$: C, 74.19; H, 5.47; N, 5.94. Found: C, 74.21; H, 5.49; N, 5.75.

**Preparation of Ligand L9.** A solution of **14** (0.30 g, 0.34 mmol), 2,6-bis(1-ethyl-5-hydroxybenzimidazol-2-yl)pyridine (0.069 g, 0.17 mmol), EDCI·HCl (0.19 g, 1.0 mmol), and DMAP (0.12 g, 1.0 mmol) in 50 mL of dry $CH_2Cl_2$ was refluxed under an atmosphere of $N_2$ for 14 h. After washing with a saturated aqueous NaCl solution (3 × 50 mL), the organic phase was dried over $Na_2SO_4$, filtered, and evaporated to dryness. Purification by column chromatography (silica; $CH_2Cl_2/CH_3OH$ = 100/0 → 98.5/1.5) gave 0.07 g (20%) of **L9**.

$^1$H NMR ($CDCl_3$): $\delta$ 8.61 (t, 2H, $^4J$ = 1.6 Hz), 8.45 (d, 2H, $^3J$ = 8.3 Hz), 8.32 (d, 4H, $^3J$ = 8.6 Hz), 8.20 (d, 4H, $^3J$ = 8.5 Hz), 8.14 (t, 1H, $^3J$ = 8.1 Hz), 7.98 (d, 4H, $^4J$ = 1.5 Hz), 7.76 (d, 2H, $^4J$ = 1.6 Hz), 7.72 (d, 8H, $^3J$ = 8.4 Hz), 7.55 (d, 2H, $^3J$ = 8.8 Hz), 7.45 (d, 8H, $^3J$ = 8.5 Hz), 7.29 (dd, 2H, $^3J$ = 8.9 Hz, $^4J$ = 1.9 Hz), 7.27 (d, 4H, $^3J$ = 8.5 Hz), 7.19 (d, 4H, $^4J$ = 2.4 Hz), 7.15 (dd, 4H, $^3J$ = 8.4 Hz, $^4J$ = 2.5 Hz), 4.83 (q, 4H, $^3J$ = 6.9 Hz), 4.38 (t, 4H, $^3J$ = 6.9 Hz), 4.13 (t, 4H, $^3J$ = 6.6 Hz), 2.29 (s, 12H), 1.75−1.92 (m, 8H), 1.42−1.57 (m, 8H), 1.43 (t, 6H, $^3J$ = 7.1 Hz), 1.31−1.42 (m, 8H). ESI-MS: *m*/*z* 2101.1 ([M + H]$^+$). Elem anal. Calcd for $C_{131}H_{113}N_9O_{18} \cdot 3.73H_2O$: C, 72.56; H, 5.60; N, 5.81. Found: C, 72.57; H, 5.58; N, 5.62.

**Preparation of Ligand L10.** A solution of 2,6-bis(1-ethyl-5-hydroxybenzimidazol-2-yl)pyridine (0.176 g, 0.44 mmol) and **15** (0.79 g, 0.88 mmol) in 50 mL of freshly distilled $CH_2Cl_2$ was cooled in an ice bath. After the addition of DCC (0.41 g, 1.99 mmol), DPTS (0.26 g, 0.88 mmol), and a spatula tip of 4-PPy, the ice bath was allowed to melt and the reaction mixture was stirred at room temperature for 16 h. The solution was filtered and evaporated to dryness. The crude product was cleaned by column chromatography (silica; $CH_2Cl_2/CH_3OH$ = 100/0 → 99/1) to yield 0.18 g (19%) of **L10**.

$^1$H NMR ($CDCl_3$): $\delta$ 8.62 (t, 2H, $^4J$ = 1.5 Hz), 8.36 (d, 2H, $^3J$ = 7.8 Hz), 8.33 (d, 4H, $^3J$ = 8.6 Hz), 8.20 (d, 4H, $^3J$ = 8.5 Hz), 8.08 (t, 1H, $^3J$ = 7.8 Hz), 7.98 (d, 4H, $^4J$ = 1.4 Hz), 7.70 (d, 2H, $^4J$ = 2.1 Hz), 7.59 (d, 4H, $^4J$ = 1.4 Hz), 7.54 (dd, 4H, $^3J$ = 7.6 Hz, $^4J$ = 1.4 Hz), 7.27 (dd, 2H, $^3J$ = 8.9 Hz, $^4J$ = 1.9 Hz), 7.25 (d, 4H, $^3J$ = 7.8 Hz), 7.19 (m, 4H), 7.11−7.17 (m, 8H), 4.82 (q, 4H, $^3J$ = 7.3 Hz), 4.38 (t, 4H, $^3J$ = 6.7 Hz), 4.13 (t, 4H, $^3J$ = 6.5 Hz), 2.13 (s, 12H), 2.07 (s, 12H), 1.77−1.92 (m, 8H), 1.41 (t, 6H, $^3J$ = 7.2 Hz), 1.31−1.57 (m, 24H). ESI-MS: *m*/*z* 2157.0 ([M + H]$^+$). Elem anal. Calcd for $C_{135}H_{121}N_9O_{18} \cdot 2.05H_2O$: C, 73.89; H, 5.75; N, 5.74. Found: C, 73.92; H, 6.01; N, 5.57.

**Preparation of Compound 29.** To a suspension of 5-(*tert*-butyldimethylsiloxy)isophthalic acid (0.70 g, 2.35 mmol) in 50 mL of freshly distilled $CH_2Cl_2$ stirred in an ice bath was added first a solution of DCC (3.00 g, 14.5 mmol), DPTS (0.30 g, 1.02 mmol), and a spatula tip of 4-PPy in 25 mL of $CH_2Cl_2$ and then a solution of **17** (2.28 g, 4.70 mmol) in 25 mL of $CH_2Cl_2$. After stirring for 30 min, the ice bath was removed and the solution was stirred for 17 h. After filtration, the solution was evaporated to dryness. The crude product was purified by column chromatography (silica; $CH_2Cl_2/CH_3OH$ = 100/0 → 99.5/0.5) to yield 2.21 g (79%) of **29**.

$^1$H NMR ($CDCl_3$): $\delta$ 8.28 (t, 1H, $^4J$ = 1.5 Hz), 8.17 (d, 4H, $^3J$ = 9.0 Hz), 7.72 (d, 4H, $^3J$ = 8.7 Hz), 7.67 (d, 4H, $^3J$ = 8.9 Hz), 7.67 (d, 2H, $^4J$ = 1.5 Hz), 7.48 (d, 2H, $^4J$ = 1.8 Hz), 7.46 (dd, 2H, $^3J$ = 8.2 Hz, $^4J$ = 2.3 Hz), 7.24 (d, 2H, $^3J$ = 8.2 Hz), 6.99 (d, 4H, $^3J$ = 8.9 Hz), 4.33 (t, 4H, $^3J$ = 6.8 Hz), 4.05 (t, 4H, $^3J$ = 6.6 Hz),

2.30 (s, 6H), 1.74−1.87 (m, 8 H), 1.30−1.53 (m, 24 H), 1.00 (s, 9H), 0.24 (s, 6H). ESI-MS: $m/z$ 1253.4 ($[M + Na]^+$). Elem anal. Calcd for $C_{76}H_{86}N_2O_{11}Si \cdot 0.33H_2O$: C, 73.75; H, 7.06; N, 2.27. Found: C, 73.75; H, 7.08; N, 2.33.

**Preparation of Compound 31.** A solution of **29** (2.24 g, 1.82 mmol) and $Zn(BF_4)_2 \cdot 6H_2O$ (8.00 g, 23.0 mmol) in 160 mL of THF and 40 mL of $H_2O$ was stirred at 60 °C for 15 h. THF was evaporated, and the aqueous phase was extracted with 4 × 40 mL of $CH_2Cl_2$. The combined organic phases were dried over $Na_2SO_4$, filtered, and evaporated. The solid residue was purified by column chromatography (silica; $CH_2Cl_2/CH_3OH$ = 100/0 → 99/1) to yield 2.01 g (99%) of **31**.

$^1$H NMR ($CDCl_3$): $\delta$ 8.26 (t, 1H, $^4J$ = 1.4 Hz), 8.17 (d, 4H, $^3J$ = 9.0 Hz), 7.72 (d, 4H, $^3J$ = 8.6 Hz), 7.70 (d, 2H, $^4J$ = 1.4 Hz), 7.67 (d, 4H, $^3J$ = 8.6 Hz), 7.48 (d, 2H, $^4J$ = 2.2 Hz), 7.45 (dd, 2H, $^3J$ = 8.2 Hz, $^4J$ = 2.3 Hz), 7.24 (d, 2H, $^3J$ = 8.3 Hz), 6.99 (d, 4H, $^3J$ = 9.0 Hz), 5.61 (s, 1H), 4.33 (t, 4H, $^3J$ = 6.7 Hz), 4.05 (t, 4H, $^3J$ = 6.6 Hz), 2.30 (s, 6H), 1.73−1.87 (m, 8 H), 1.30−1.53 (m, 24 H). ESI-MS: $m/z$ 1116.1 ($[M - H]^-$). Elem anal. Calcd for $C_{70}H_{72}N_2O_{11} \cdot 0.18H_2O$: C, 75.02; H, 6.51; N, 2.51. Found: C, 75.02; H, 6.58; N, 2.43.

**Preparation of Compound 33.** To a solution of 4-(10-hydroxydecyloxy)benzoic acid (0.53 g, 1.79 mmol) in 100 mL of freshly distilled $CH_2Cl_2$ stirred in an ice bath was added **31** (2.00 g, 1.79 mmol), DPTS (0.53 g, 1.79 mmol), DCC (0.83 g, 4.00 mmol), and a spatula tip of 4-PPy. The ice bath was removed, and the solution was stirred at room temperature for 72 h. After filtration, the solution was evaporated to dryness and the crude product was purified by column chromatography (silica; $CH_2Cl_2/CH_3OH$ = 100/0 → 99/1) to yield 2.44 g (98%) of **33**.

$^1$H NMR ($CDCl_3$): $\delta$ 8.60 (t, 1H, $^4J$ = 1.4 Hz), 8.17 (d, 4H, $^3J$ = 9.0 Hz), 8.14 (d, 2H, $^3J$ = 9.0 Hz), 8.06 (d, 2H, $^4J$ = 1.4 Hz), 7.72 (d, 4H, $^3J$ = 9.0 Hz), 7.67 (d, 4H, $^3J$ = 9.0 Hz), 7.48 (d, 2H, $^4J$ = 2.3 Hz), 7.45 (dd, 2H, $^3J$ = 8.7 Hz, $^4J$ = 2.3 Hz), 7.24 (d, 2H, $^3J$ = 8.4 Hz), 6.98 (d, 6H, $^3J$ = 8.7 Hz), 4.35 (t, 4H, $^3J$ = 6.6 Hz), 4.04 (t, 6H, $^3J$ = 6.6 Hz), 3.64 (t, 2H, $^3J$ = 6.5 Hz), 2.30 (s, 6H), 1.74−1.86 (m, 10 H), 1.54−1.61 (m, 2 H), 1.29−1.52 (m, 36 H). ESI-MS: $m/z$ 1411.1 ($[M + H_2O]^+$). Elem anal. Calcd for $C_{87}H_{96}N_2O_{14} \cdot 0.64H_2O$: C, 74.36; H, 6.98; N, 1.99. Found: C, 74.36; H, 7.14; N, 2.20.

**Preparation of Compound 35.** To a solution of 4-carboxybenzaldehyde (74 mg, 0.49 mmol) and **33** (670 mg, 0.49 mmol) in 100 mL of freshly distilled $CH_2Cl_2$ stirred in an ice bath was added DPTS (30 mg, 0.10 mmol), DCC (300 mg, 1.45 mmol), and a spatula tip of 4-PPy. After 30 min, the ice bath was removed and the solution was stirred for 24 h at room temperature. The solution was filtered and evaporated, and the crude product was purified by column chromatography (silica; $CH_2Cl_2/CH_3OH$ = 100/0 → 99.5/0.5) to yield 700 mg (96%) of **35**.

$^1$H NMR ($CDCl_3$): $\delta$ 10.10 (s, 1H) 8.59 (t, 1H, $^4J$ = 1.5 Hz), 8.20 (d, 2H, $^3J$ = 8.4 Hz), 8.17 (d, 4H, $^3J$ = 8.9 Hz), 8.14 (d, 2H, $^3J$ = 9.0 Hz), 8.06 (d, 2H, $^4J$ = 1.6 Hz), 7.95 (d, 2H, $^3J$ = 8.3 Hz), 7.72 (d, 4H, $^3J$ = 8.6 Hz), 7.67 (d, 4H, $^3J$ = 8.5 Hz), 7.48 (d, 2H, $^4J$ = 2.3 Hz), 7.46 (dd, 2H, $^3J$ = 8.4 Hz, $^4J$ = 2.3 Hz), 7.24 (d, 2H, $^3J$ = 8.4 Hz), 6.99 (d, 4H, $^3J$ = 8.9 Hz), 6.98 (d, 2H, $^3J$ = 9.0 Hz), 4.36 (t, 2H, $^3J$ = 6.7 Hz), 4.35 (t, 4H, $^3J$ = 6.7 Hz), 4.05 (t, 6H, $^3J$ = 6.5 Hz), 2.30 (s, 6H), 1.74−1.87 (m, 12 H), 1.30−1.52 (m, 36 H). ESI-MS: $m/z$ 1543.1 ($[M + H_2O]^+$). Elem anal. Calcd for $C_{95}H_{100}N_2O_{16} \cdot 0.91H_2O$: C, 73.98; H, 6.65; N, 1.82. Found: C, 73.98; H, 6.60; N, 1.86.

**Preparation of Compound 37.** A solution of **35** (0.64 g, 0.42 mmol), $NaClO_2$ (0.20 g, 2.2 mmol), and $H_2NSO_3H$ (0.21 g, 2.3 mmol) in 25 mL of THF and 25 mL of $H_2O$ was stirred at room temperature for 2 h. After evaporation of THF, the aqueous phase was extracted with 2 × 50 mL of $CH_2Cl_2$. The combined organic phases were dried over $Na_2SO_4$, filtered, and evaporated to yield 0.64 g (99%) of **37**.

$^1$H NMR ($CDCl_3$): $\delta$ 8.59 (t, 1H, $^4J$ = 1.5 Hz), 8.11−8.19 (m, 10H), 8.06 (d, 2H, $^4J$ = 1.5 Hz), 7.72 (d, 4H, $^3J$ = 8.6 Hz), 7.67 (d, 4H, $^3J$ = 8.6 Hz), 7.48 (d, 2H, $^4J$ = 2.2 Hz), 7.46 (dd, 2H, $^3J$ = 8.3 Hz, $^4J$ = 2.2 Hz), 7.24 (d, 2H, $^3J$ = 8.3 Hz), 6.98 (d, 4H, $^3J$ = 9.0 Hz), 6.98 (d, 2H, $^3J$ = 9.0 Hz), 4.35 (t, 6H, $^3J$ = 6.7 Hz), 4.04 (t, 6H, $^3J$ = 6.6 Hz), 2.30 (s, 6H), 1.74−1.89 (m, 12 H), 1.29−1.53 (m, 36 H). ESI-MS: $m/z$ 1540.3 ($[M - H]^-$). Elem anal. Calcd for $C_{95}H_{100}N_2O_{17} \cdot 1.92H_2O$: C, 72.38; H, 6.64; N, 1.78. Found: C, 72.38; H, 6.75; N, 1.70.

**Preparation of Ligand L6.** A solution of **37** (1.46 g, 0.95 mmol), 2,6-bis(1-ethyl-5-hydroxybenzimidazol-2-yl)pyridine (189 mg, 0.47 mmol), EDCI·HCl (400 mg, 2.1 mmol), and DMAP (250 mg, 2.05 mmol) in 100 mL of freshly distilled $CH_2Cl_2$ was refluxed under $N_2$ for 17 h. The solution was extracted three times with 80 mL of $H_2O$ + 10 mL of saturated $NH_4Cl$. The combined aqueous phases were extracted with 50 mL of $CH_2Cl_2$, and the organic extracts were dried over $Na_2SO_4$, filtered, and evaporated to dryness. The crude product was purified by column chromatography (silica; $CH_2Cl_2/CH_3OH$ = 100/0 → 99/1). Yield: 830 mg (51%).

$^1$H NMR ($CDCl_3$): $\delta$ 8.59 (t, 2H, $^4J$ = 1.5 Hz), 8.35 (d, 2H, $^3J$ = 8.1 Hz), 8.33 (d, 4H, $^3J$ = 8.6 Hz), 8.20 (d, 4H, $^3J$ = 8.5 Hz), 8.16 (d, 8H, $^3J$ = 8.9 Hz), 8.14 (d, 4H, $^3J$ = 8.8 Hz), 8.08 (t, 1H, $^3J$ = 7.9 Hz), 8.05 (d, 4H, $^4J$ = 1.5 Hz), 7.72 (d, 8H, $^3J$ = 8.4 Hz), 7.71 (d, 2H, $^4J$ = 2.3 Hz), 7.67 (d, 8H, $^3J$ = 8.4 Hz), 7.52 (d, 2H, $^3J$ = 9.0 Hz), 7.48 (d, 4H, $^4J$ = 2.1 Hz), 7.46 (dd, 4H, $^3J$ = 8.3 Hz, $^4J$ = 2.2 Hz), 7.25 (dd, 2H, $^3J$ = 9.0 Hz, $^4J$ = 2.3 Hz), 7.24 (d, 4H, $^3J$ = 8.3 Hz), 6.98 (d, 12H, $^3J$ = 9.0 Hz), 4.82 (q, 4H, $^3J$ = 7.2 Hz), 4.38 (t, 4H, $^3J$ = 6.7 Hz), 4.35 (t, 8H, $^3J$ = 6.8 Hz), 4.05 (t, 4H, $^3J$ = 6.6 Hz), 4.04 (t, 8H, $^3J$ = 6.6 Hz), 2.30 (s, 12H), 1.74−1.87 (m, 24 H), 1.30−1.52 (m, 78 H). ESI-MS: $m/z$ 1724.3 ($[M + 2H]^{2+}$). Elem anal. Calcd for $C_{213}H_{217}N_9O_{34} \cdot 0.22H_2O$: C, 74.13; H, 6.35; N, 3.65. Found: C, 74.14; H, 6.41; N, 3.53.

**Preparation of $[Ln(L\boldsymbol{k})(NO_3)_3] \cdot n\boldsymbol{H_2O}$ Complexes.** In a typical preparation, 100−150 mg of ligand (**L*k***) was dissolved in 5 mL of $CH_2Cl_2$. A total of 1 equiv of $Ln(NO_3)_3 \cdot nH_2O$ (Ln = Y, La, Pr, Eu, Gd, Tb, Lu) in 5 mL of $CH_3CN$ was added, and the solution was stirred for 1 h. After evaporation of the solvent, the complex was washed with $CH_3CN$ and dried in a vacuum overnight at 60 °C. Yields ranged from 72 to 89%. Elemental analyses were collected in Table S1 (Supporting Information)

**Spectroscopic and Analytical Measurements.** $^1$H NMR spectra were recorded at 25 °C on a Bruker Avance 400 MHz spectrometer. Chemical shifts are given in ppm with respect to tetramethylsilane. Diffusion experiments were carried out at 400 MHz Larmor frequency. Solutions ($CD_2Cl_2$, 293 K, $|complex|_{tot}$ = $10^{-2}$ M) of the complex were prepared in situ and left to equilibrate for 48 h. The pulse sequence used was the Bruker pulse program *ledbpgp2s*,[38] which employs stimulated echo, bipolar gradients, and longitudinal eddy current delay as the $z$ filter. The four 2 ms gradient pulses have sine-bell shapes and amplitudes ranging linearly from 2.5 to 50 G·cm$^{-1}$ in 32 steps. The diffusion delay was in the range 60−140 ms depending on the analyte diffusion coefficient, and the number of scans was 32. Processing was done using a line broadening of 5 Hz, and the diffusion coefficients were calculated with the Bruker processing package. VT-NMR measurements of samples (5−20 mg; $c \approx 10^{-2}$ M) in a $CD_2Cl_2$ solution were measured on a Bruker Avance 400 spectrometer equipped with a variable-temperature unit. The integrated intensities of the relevant peaks were obtained by deconvolution using Matlab or Excel (one Lorentz function per peak) after Fourier transformation and phasing of the spectrum using *SpinWorks*. Fitting of van't Hoff plots was done using Excel. The standard deviations of $\Delta G$, $K$, and $T_{50\%}$ were calculated by taking into account the strong interdependence of the values of $\Delta H$ and $\Delta S$, derived from the slope and intercept, respectively, of the van't Hoff plots. The covariance matrix of $\Delta H$ and $\Delta S$ was calculated with the macro *LS1*, and the standard deviations

(38) Wu, D.; Chen, A.; Johnson, C. S., Jr. *J. Magn. Reson. A* **1995**, *115*, 260–264.

of the other three parameters were calculated using the macro *Propagation*.[21] Pneumatically assisted ESI-MS spectra were recorded from $10^{-4}$ M solutions on an Applied Biosystems API 150EX LC/MS system equipped with a Turbo Ionspray source. Elemental analyses were performed by Dr. H. Eder from the Microchemical Laboratory of the University of Geneva. TGA was performed with a Seiko TG/DTA 320 thermogravimetric balance(under $N_2$). DSC traces were obtained with a Mettler Toledo DSC1 Star Systems differential scanning calorimeter from 3 to 5 mg samples (5 °C·min$^{-1}$, under $N_2$). Characterization of the mesophases was performed with a Leitz Orthoplan-Pol polarizing microscope with a Leitz LL 20×/0.40 polarizing objective and equipped with a Linkam THMS 600 variable-temperature stage. The SA-XRD patterns were obtained with four different experimental setups, and in all cases, the crude powder was filled in Lindemann capillaries of 1 mm diameter. (1) A STOE STADI P transmission powder diffractometer system using a focused monochromatic Cu K$\alpha_1$ beam obtained from a curved germanium monochromator (Johann-type) and collected on a curved image-plate position sensitive detector. A calibration with silicon and copper laurate standards, for high- and low-angle domains, respectively, was preliminarily performed. Sample capillaries were placed in the high-temperature attachment for measurements in the range of desired temperatures (from −40 to +170 °C) within ±0.05 °C. Periodicities up to 50 Å could be measured. The exposure times were varied from 1 to 4 h. (2) An Inel CPS 120 curved counter using a linear monochromatic Cu K$\alpha_1$ beam obtained with a sealed-tube generator (900 W) and a bent quartz monochromator, for which the sample temperature was controlled within ±0.05 °C. Periodicities up to 60 Å could be measured. (3) An image plate. The cell parameters were calculated from the position of the reflection at the smallest Bragg angle, which was in all cases the most intense. Periodicities up to 90 Å could be measured, and the sample temperature was controlled within ±0.3 °C. The exposure times were varied from 1 to 24 h, depending on the specific reflections being sought (weaker reflections obviously taking longer exposure times). (4) A SAXS system from Molecular Metrology equipped with a Cu Kα Bede microsource conditioned with confocal Max-FluxTM optics and a two-dimensional multiwire gas detector. A modified temperature stage from Linkham was used to control the temperatures. The analysis was performed with MatLab-based open-source software from Molecular Metrology.

**Acknowledgment.** The authors acknowledge contributions of the Sciences Mass Spectrometry platform at the Faculty of Sciences, University of Geneva, for mass spectrometry services. Financial support from the Swiss National Science Foundation is gratefully acknowledged.

**Supporting Information Available:** Tables of elemental analyses (Table S1) and SA-XRD data (Tables S2 and S3) for complexes [Ln(***Lk***)$(NO_3)_3$], schemes for the syntheses of ligands **L7**−**L14** (Schemes S1 and S2), and figures showing van't Hoff analyses (Figures S1−S3), TGA and DSC traces (Figures S4, S8, S9, and S13), birefringent textures (Figures S5 and S10), SA-XRD profiles (Figures S7, S10, S12, S14, and S15), and molecular modeling of the complexes [Ln(***Lk***)$(NO_3)_3$] (Figure S11). This material is available free of charge via the Internet at http://pubs.acs.org.